

CHEMISTRY

A European Journal



Accepted Article

Title: Unusual Magneto-structural Features of the Halo-Substituted Materials

[FeIII(5-X-salMeen)2]Y: a Cooperative [HS-HS] ↔ [HS-LS] Spin Transition

Authors: Musa Sipho Shongwe, Mariam Al-Azzani, Faizah Al-Mjeni, Ryoji Mitsuhashi, Masahiro Mikuriya, Craig Robertson, Imaddin Al-Omari, and Eckhard Bill

This manuscript has been accepted after peer review and appears as an Accepted Article online prior to editing, proofing, and formal publication of the final Version of Record (VoR). This work is currently citable by using the Digital Object Identifier (DOI) given below. The VoR will be published online in Early View as soon as possible and may be different to this Accepted Article as a result of editing. Readers should obtain the VoR from the journal website shown below when it is published to ensure accuracy of information. The authors are responsible for the content of this Accepted Article.

To be cited as: *Chem. Eur. J.* 10.1002/chem.201904744

Link to VoR: <http://dx.doi.org/10.1002/chem.201904744>

Supported by
ACES

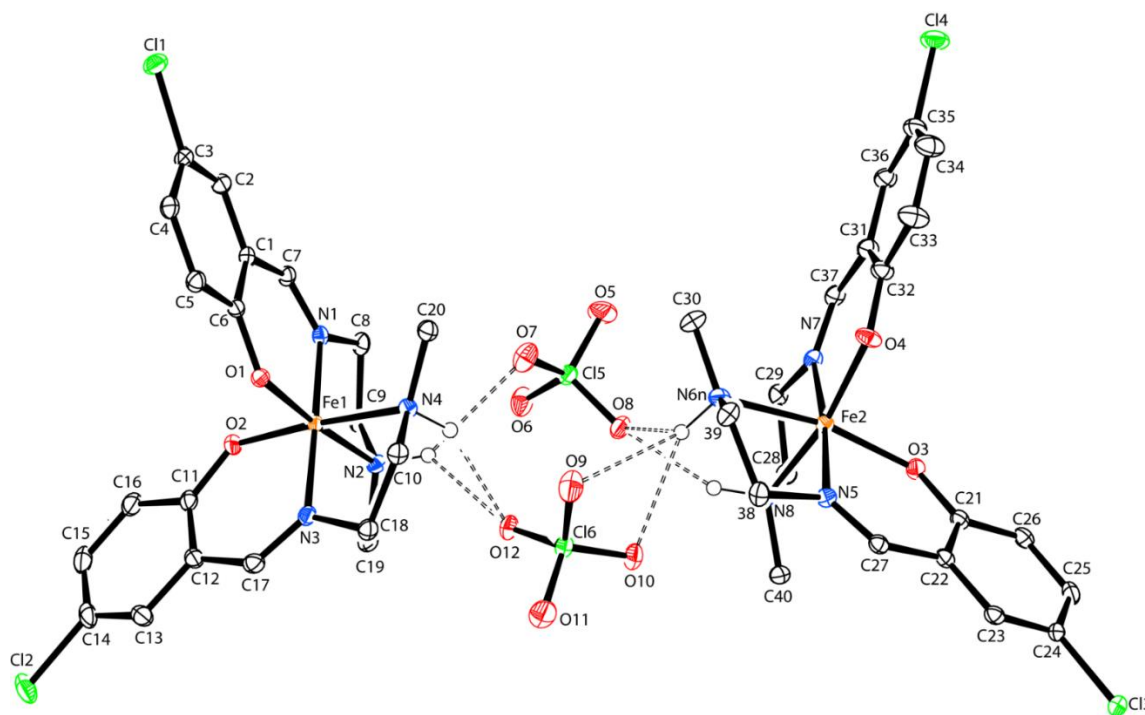
WILEY-VCH

Unusual Magneto-structural Features of the Halo-Substituted Materials [Fe^{III}(5-X-salMeen)₂Y]: a Cooperative [HS-HS] ↔ [HS-LS] Spin Transition

Mariam A. Al-Azzani,^[a] Faizah Al-Mjeni,^[a] Ryoji Mitsuhashi,^[b] Masahiro Mikuriya,^[b] Imad Al-Omari,^[c] Craig C. Robertson,^[d] Eckhard Bill,^[e] Musa S. Shongwe*^[a]

Graphical Abstract

Unusual spin-crossover features of [Fe^{III}(5-X-salMeen)₂]⁺: The series of compounds [Fe^{III}(5-X-salMeen)₂]ClO₄ (X = a halogen substituent) exhibit 50% spin crossover with a broad [HS-LS] plateau, a magnetic profile hitherto not crystallographically elucidated within the Fe^{III}-salRen family (R = alkyl group). As its solvated BPh₄⁻ salt, [Fe^{III}(5-Cl-salMeen)₂]⁺ is LS and undergoes a temperature-dependent crystallographic phase transition.



Keywords

Ferric spin crossover · spin-transition plateau · noncovalent interactions · crystallographic phase transition · electronic and electrochemical processes

Ferric Spin Crossover**Unusual Magneto-structural Features of the Halo-Substituted Materials
[Fe^{III}(5-X-salMeen)₂]Y: a Cooperative [HS-HS] ↔ [HS-LS] Spin Transition**

Mariam A. Al-Azzani,^[a] Faizah Al-Mjeni,^[a] Ryoji Mitsuhashi,^[b] Masahiro Mikuriya,^[b] Imad Al-Omari,^[c] Craig C. Robertson,^[d] Eckhard Bill,^[e] Musa S. Shongwe,^{*[a]}

[a] *M. A. Al-Azzani, Dr. F. Al-Mjeni, Prof. M. S. Shongwe*
Department of Chemistry, College of Science, Sultan Qaboos University, Private Bag 36, Al-Khod 123, Muscat
(Sultanate of Oman)
E-mail: musa@squ.edu.om

[b] *Dr. R. Mitsuhashi, Prof. M. Mikuriya*
School of Science and Technology, Kwansai Gakuin University, 2-1 Gakuen, Sanda 669-1337 (Japan)

[c] *Prof. I. Al-Omari*
Department of Physics, College of Science, Sultan Qaboos University, Private Bag 36, Al-Khod 123, Muscat
(Sultanate of Oman)

[d] *Dr. C. C. Robertson*
Department of Chemistry, University of Sheffield, Sheffield S3 7HF (United Kingdom)

[e] *Dr. E. Bill*
Max-Planck-Institut für Chemische Energiekonversion, Stiftstrasse 34-36, D-45470, Mülheim an der Ruhr (Germany)

Abstract:

X-ray structures of the halo-substituted complexes [Fe^{III}(5-X-salMeen)₂]ClO₄ (X = F, Cl, Br, I) at RT have revealed the presence of two discrete HS complex cations in the crystallographic asymmetric unit with two perchlorate counter ions linking them by N–H_{amine}⋯O_{perchlorate} interactions. At 90 K, the two complex cations are distinctly HS and LS, a rare crystallographic observation of this coexistence in the Fe^{III}-salRen spin-crossover (SCO) system. At both temperatures, crystal packing shows dimerization through C–H_{imine}⋯O_{phenolate} interactions, a key feature for SCO cooperativity. Moreover, there are noncovalent contacts between the complex cations through type-II halogen-halogen bonds, which are novel in this system. The magnetic profiles and Mössbauer spectra concur with the structural analyses and reveal 50% SCO of the type [HS-HS] ↔ [HS-LS] with a broad plateau. In contrast, [Fe^{III}(5-Cl-salMeen)₂]BPh₄·2MeOH is LS and exhibits a temperature-dependent crystallographic phase transition, exemplifying the influence of lattice solvents and counter ions on SCO.

Introduction

Virtually four decades ago the first example of an abrupt hysteretic ${}^6A_1 \leftrightarrow {}^2T_2$ spin-crossover complex, *viz.* $[\text{Fe}^{\text{III}}(\text{3-OMe-salEen})_2]\text{PF}_6$,^[1] within the family of mononuclear iron(III) salicylaldimines $[\text{Fe}^{\text{III}}(\text{R}^1, \text{R}^2\text{-salRen})_2]^+$, was reported and its crystallographic analysis^[2] was performed three decades later. It was not until very recently that the literature witnessed two other salEen-based examples of SCO materials exhibiting an abrupt spin transition with hysteresis, *viz.* $[\text{Fe}^{\text{III}}(\text{4-OMe-salEen})_2]\text{NO}_3$ ^[3] and $[\text{Fe}^{\text{III}}(\text{5-Br-salEen})_2]\text{ClO}_4$.^[4] Indeed, in general, there is a paucity of iron(III) spin-crossover complexes that display the much sought-after unique spin-transition features such as abrupt and hysteretic,^[1-15] symmetry-breaking,^[16-18] stepwise and wide [HS-LS] plateau^[5,6,16-20] and structural phase transition,^[21] attributable to cooperativity amongst the paramagnetic centres in the crystal lattice via noncovalent intermolecular forces. Within the $[\text{Fe}^{\text{III}}(\text{R}^1, \text{R}^2\text{-salRen})_2]^+$ system, observation of cooperative spin crossover is even rarer. The impetus for spin-crossover research derives from the potential technological applications^[22,23] of magnetically bistable molecular materials in the fabrication of electronic devices as well as the sheer scientific interest in designing and generating complexes with fascinating magneto-structural properties. Crucial criteria for spin crossover to materialize in octahedral complexes are: (1) a first-row transition-metal ion with a d^4 – d^7 ground-state electron configuration, and (2) a coordination donor-atom set that provides a ligand-field strength capable of stabilizing either spin state of the central metal ion as dictated by external perturbations. A spin transition is triggered principally by temperature, pressure and electromagnetic radiation.

The concerted groundbreaking investigation of the spin-crossover curiosities in the series of complexes $[\text{Fe}^{\text{III}}(\text{R}^1, \text{R}^2\text{-salRen})_2]\text{Y}$ by Hendrickson, Sinn, Wilson *et al.*^[1,21,24-28] revealed *inter alia* the subtle effects of ligand substituent groups, counter ions, lattice solvents, intermolecular forces and sample type on the nature of spin-state transformations. The tridentate *en*-based salicylaldimine ligands of considerable interest were H-R¹-salRen (R = Et, H-R¹-salEen; Me, H-R¹-salMeen and Bz, H-R¹-salBzen), with the substituent groups R¹ (commonly –OMe, –OEt and –NO₂) in either the *ortho* or *para* positions of the phenolate moiety. Just over a decade ago, this system was extended to the Schiff-base ligands H-R¹-salPen and H-R¹-salBen (R = *n*-propyl and *n*-butyl, respectively).^[29]

Modulation of spin-crossover properties in iron(III)-salicylaldimine systems by introducing halogen substituents into the *para* position of the phenolate moiety has been demonstrated spectacularly by the complexes $[\text{Fe}(\text{qsal-5-X})_2]\text{Y}$ (X = halogen; Y ; counter ion).^[6,7,11,18,30] Within the family $[\text{Fe}^{\text{III}}(\text{R}^1, \text{R}^2$

salRen)₂Y, only three crystallographically characterized 5-halo-substituted members are known, namely [Fe^{III}(5-Br-salEen)₂]Cl·½H₂O,^[31] [Fe^{III}(5-Br-salEen)₂]ClO₄,^[4,32] and [Fe^{III}(5-I-salEen)₂]ClO₄.^[33] [Fe^{III}(5-Br-salEen)₂]Cl·½H₂O exists at 150 K as two independent complex cations in the crystallographic asymmetric unit: one in the HS state and the other in the LS state, a magnetic feature not crystallographically observed previously in this system. However, structural evidence of such [HS-LS] coexistence has been reported for a mere handful of other types of iron(III)-based SCO complexes,^[5,16–18,20,30,31,34,35] generally those whose spin transition exhibits a [HS-LS] plateau. Unfortunately, room-temperature magnetic and crystallographic data on [Fe^{III}(5-Br-salEen)₂]Cl·½H₂O^[31] are not available, nor a spin-transition curve for this compound. [Fe^{III}(5-Br-salEen)₂]ClO₄,^[4,32] exhibits polymorphism induced by the crystallization conditions. The polymorph that crystallizes in the monoclinic space group *P*2₁/*c*^[4] undergoes an abrupt complete *S* = 5/2 ↔ *S* = 1/2 crossover involving one complex cation whereas the other polymorph which adopts the orthorhombic space group *Pbcn*^[32] is predominantly low spin at room temperature, and its incomplete spin crossover is characterized by an asymmetric hysteresis loop around room temperature. The magneto-structural behaviour of the 5-iodo-substituted analogue^[33] has a striking resemblance to that of the latter polymorph save for the irreversibility of the magnetic profile and the narrower hysteresis loop in this case.

The object of this work is to revisit the [Fe^{III}(X-salRen)₂]Y spin-crossover family^[24,26] that originated in the 1970s and extend it with freshly designed members that have the potential to exhibit previously unobserved rare magnetic behaviour. In the course of this investigation, some aspects of our work coincided with the research conducted by Martinho *et al.*^[4,31–33] Herein we present a report on a systematic study of spin-crossover features within the series of halo-substituted complexes [Fe^{III}(5-X-salMeen)₂]Y (X = F, Cl, Br and I; Y = ClO₄ and BPh₄). Previously, Wilson and Sinn along with their co-workers demonstrated magnetically and crystallographically the influence of electronic properties of substituent groups on the spin states of the compounds in the series [Fe^{III}(X-salMeen)₂]PF₆ (X = 5-OMe, 3-OMe and 5-NO₂).^[24,26] In our work the magneto-structural properties of [Fe^{III}(5-X-salMeen)₂]ClO₄ (X = halogen) reveal a thermally induced [HS-HS] ↔ [HS-LS] spin transition with a broad [HS-LS] plateau, a highly unusual magnetic feature in this iron(III)-salicylideneamine spin-crossover system.

Furthermore, in the compounds [Fe^{III}(5-X-salMeen)₂]ClO₄ (X = Cl, Br, I) we have encountered halogen-halogen bonding, which is a dominant feature of the structures. To the best of our knowledge,

hitherto there has been no crystallographic documentation of the occurrence of halogen-halogen bonding^[36-41] within the $[\text{Fe}^{\text{III}}(\text{X-salRen})_2]\text{Y}$ spin-crossover family. Halogen-halogen bonds ($\text{C}_1-\text{X}_1\cdots\text{X}_2-\text{C}_2$, $\text{X} = \text{halogen}$) are categorized as types I and II. Geometrically, these types are readily distinguishable by their characteristic angles θ_1 and θ_2 :^[36,37,39-41] whereas for type-I interactions, θ_1 and θ_2 are obtuse and nearly equivalent; for type-II contacts, θ_1 and θ_2 are comparable with the idealized linear and right angles, respectively. Chemically, the type-II halogen-halogen bond differs from that of type-I in that it is electrostatic in nature ($\text{C}-\text{X}^{\delta+}\cdots\text{X}^{\delta-}-\text{C}$), i.e. electrophilic (positive “ σ -hole”)/nucleophilic interaction, and the order of prevalence is $\text{Cl} < \text{Br} < \text{I}$ in accordance with the polarizability of the halogen atom.^[37,41]

A comparison of the structural analyses of the compounds $[\text{Fe}^{\text{III}}(5\text{-Cl-salMeen})_2]\text{ClO}_4$ (**2**) and $[\text{Fe}^{\text{III}}(5\text{-Cl-salMeen})_2]\text{BPh}_4\cdot 2\text{MeOH}$ (**5·2MeOH**) illustrates the combined influence of intermolecular forces and crystal packing on the magneto-structural properties of SCO materials. Recently, a π -conjugated photo-isomerizable azo-phenyl substituent^[42] was introduced in the *para*-position of the phenolic structural moiety of the salEen ligand to diversify and maximize the noncovalent interactions, leading to thermally stable iron(III) complexes exhibiting high-temperature spin transitions. In another study, SCO in the compound $[\text{Fe}(3\text{-OMe-salEen})_2][\text{Ni}(\text{dmit})_2]\cdot\text{MeOH}$ and the non-solvated compound $[\text{Fe}(3\text{-OMe-salEen})_2][\text{Ni}(\text{dmit})_2]$ ($\text{dmit}^{2-} = 2\text{-thioxo-1,3-dithiole-4,5-dithiolato}$) occurred with $T_{1/2}$ values of 345 and 275 K, respectively, with the latter compound having lost noncovalent interactions involving the solvent.^[43]

Results and Discussion

Synthetic Strategy and Verification of Chemical Identities

The multifaceted structural design of the compounds of the type $[\text{Fe}^{\text{III}}(3,5\text{-R}^1, \text{R}^2\text{-salRen})]\text{Y}$ necessitates syntheses and isolation of a diverse range of materials to be investigated for SCO behaviour. Thus it is convenient and cost-effective to produce each iron(III)-salicylideneamine compound in a short one-pot two-step process that entails generating the ligand by Schiff-base condensation reaction with subsequent complexation of the ferric ion *in situ*. In this work, equimolar amounts of *N*-methylethylenediamine and the appropriate *para*-halo-substituted salicylaldehyde reacted instantaneously to afford the desired Schiff base 5-X-HsalMeen ($\text{X} = \text{F}, \text{Cl}, \text{Br}$ or I), but the reaction mixture was heated under reflux to maximize the yield. In general, in previous studies the ligands 3,5- R^1, R^2 -HsalRen have been employed merely as intermediate substances in the fabrication

of SCO materials. In this work, 5-I-HsalMeen (Figure 1) was selected for spectroscopic characterization and was isolated as an orange-yellow powder; the low yield ($\sim 0.8\%$) underscores the necessity to generate and utilize these ligands *in situ*. The Schiff-base imine bond in this ligand is characterized by the stretching frequency 1627 cm^{-1} in the IR spectrum and the broad visible $\pi \rightarrow \pi^*$ absorption band ($\lambda_{\text{max}} \sim 420\text{ nm}$) in the electronic absorption spectrum, which disappears upon reduction with BH_4^- .

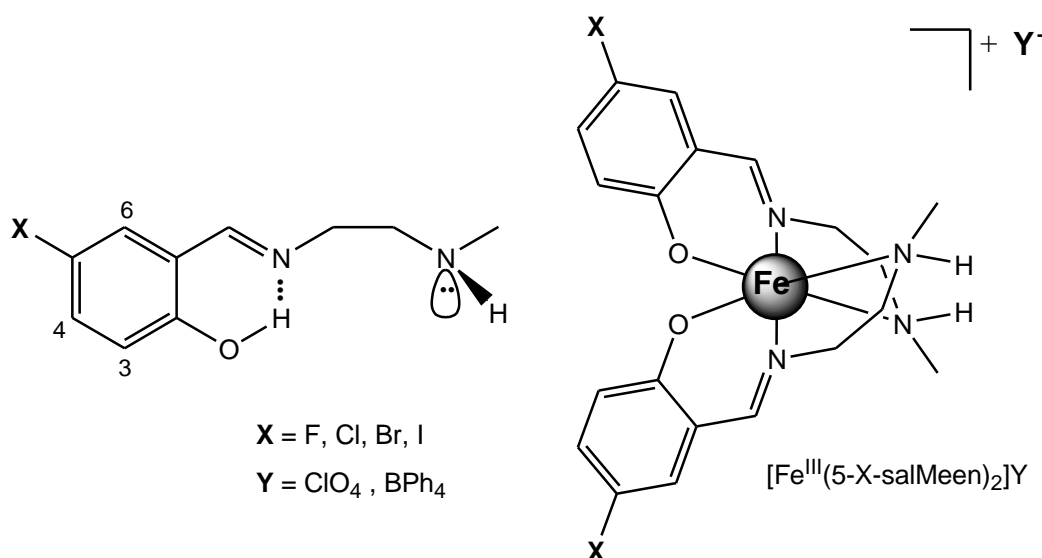


Figure 1. Designations of Schiff-base ligands and their corresponding complexes

The best $^1\text{H-NMR}$ spectrum of 5-I-HsalMeen is that recorded in $\text{DMSO-}d_6$ at a radiofrequency of 700 MHz, even though some of the aliphatic proton resonances coincide with those of the solvent; a portion of the spectrum is displayed in Figure S1. The azomethine proton ($-\text{CH}=\text{N}-$) is associated with the singlet at $\delta 8.56$. The most deshielded proton is that of the phenolic $-\text{OH}$ group with a chemical shift of $\delta 13.47$; crystallographic elucidation of closely related salicylaldimine-based Schiff bases invariably shows H-bonding interaction between the phenolic proton and the imine nitrogen.^[44,45] The resonances at $\delta 7.78$ (d; $J = 2.31\text{ Hz}$), $\delta 7.59$ (dd; $J = 8.68, 2.31\text{ Hz}$) and $\delta 6.72$ (d; $J = 8.61\text{ Hz}$) are ascribable to the aromatic protons H^6 , H^4 and H^3 (Figure 1), respectively, consistent with the *para*-substitution of the phenolic ring.

Treatment of each of the ligands 5-X-HsalMeen with half a molar equivalent of $\text{Fe}(\text{ClO}_4)_3 \cdot x\text{H}_2\text{O}$ produced the compounds $[\text{Fe}^{\text{III}}(5\text{-X-salMeen})_2]\text{ClO}_4$ (**1–4**), which were isolated as black needles upon crystallization from the intense purple solutions in methanol. In the case of $[\text{Fe}^{\text{III}}(5\text{-Cl-}$

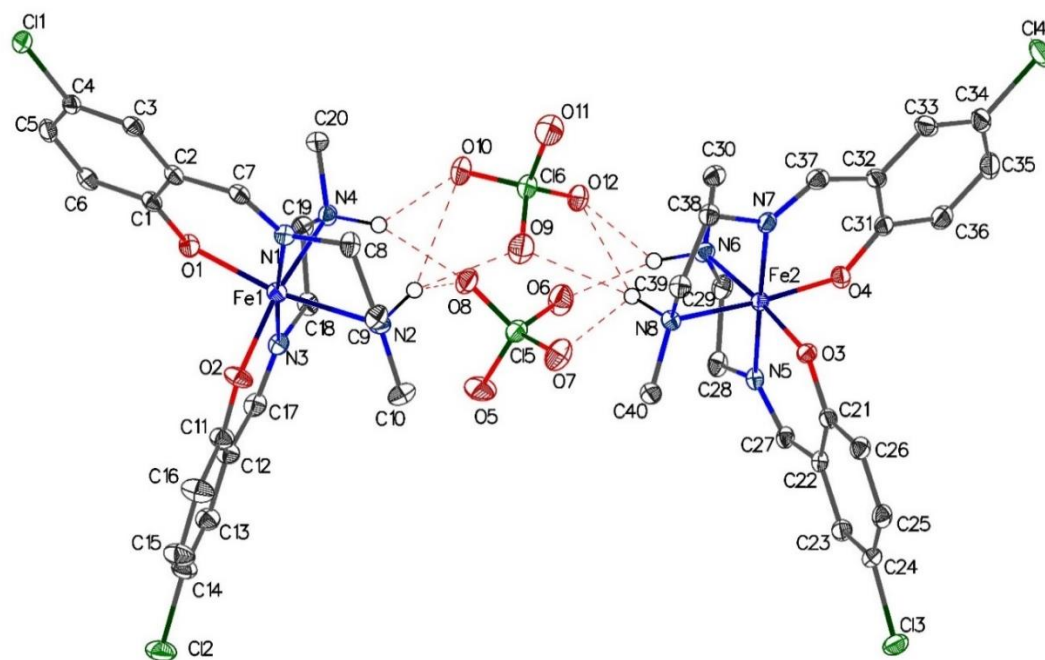
salMeen)₂]BPh₄·2MeOH (**5·2MeOH**), the ferric iron was introduced as its chloride salt and the tetraphenylborate ion as its sodium salt in three-fold molar excess. The chemical compositions and structural formulations of the iron(III)-salicylideneamine compounds (Figure 1) were established by microanalyses (CHN), mass spectrometry, molar conductivity measurements, vibrational spectroscopy and single-crystal X-ray crystallography. Characteristic IR absorption bands for the imine (C=N) and secondary amine (N–H) bonds occur in the ranges 1620–1635 and 3130–3330 cm⁻¹, respectively. Conspicuously, the ClO₄⁻ counter ion appears as strong vibrations in the range 1180–1060 cm⁻¹ accompanied by a moderate one at 625 cm⁻¹.^[34a,45–47] The presence of the BPh₄⁻ counter ion and the solvent molecules of crystallization in [Fe^{III}(5-Cl-salMeen)₂]BPh₄·2MeOH was evidenced by the stretching frequencies 730, 710 and 605 cm⁻¹^[45,47] for the former and a broad absorption band at 3480 cm⁻¹ corresponding to the latter.

Single-Crystal X-ray Analyses of X-salMeen-Based Iron(III) Complexes

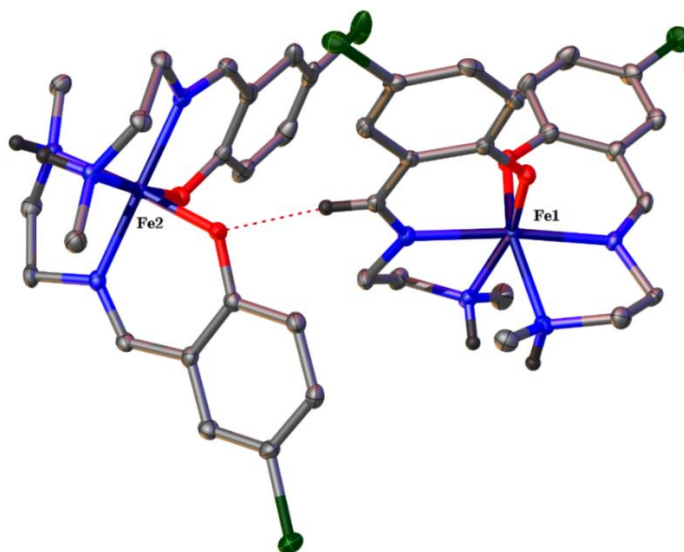
Temperature dependence of the X-ray structures of members of the series [Fe^{III}(5-X-salMeen)₂]ClO₄ (X = F, Cl, Br and I) (**1–4**) along with the compound [Fe^{III}(5-Cl-salMeen)₂]BPh₄·2MeOH (**5·2MeOH**) was investigated to gain an insight into the magnetochemistry of these materials. Selected crystallographic data for **1–4** and **5·2MeOH** are compiled in Tables 1 and 2, respectively.

*X-ray structures of [Fe^{III}(5-X-salMeen)₂]ClO₄ (X = F, Cl, Br, I) (**1–4**)*

For all the iron(III)-5-X-salMeen compounds, but [Fe^{III}(5-Cl-salMeen)₂]ClO₄, X-ray diffraction data were collected on a crystal from the same sample at 298 and 90 K (Tables 1 and 2). Compounds **1–4** crystallized as needles in the monoclinic space group *P2₁/n* (*Z* = 8) independent of the temperature of measurement. On the whole, these iron(III) compounds are isostructural; hence the same atom numbering scheme has been adopted. The crystallographic asymmetric unit for each of these compounds at both temperatures of data collection comprises two discrete complex cations with two perchlorate counter ions in between connecting them with N–H_{amine}⋯O_{perchlorate} hydrogen-bonding interactions (Tables S1–S4) as illustrated in Figures 2 and 3 for complex **2**.



(a)



(b)

Figure 2. (a) An asymmetric unit and (b) a dimer of $[\text{Fe}^{\text{III}}(5\text{-Cl-salMeen})_2]\text{ClO}_4$ at 90 K.

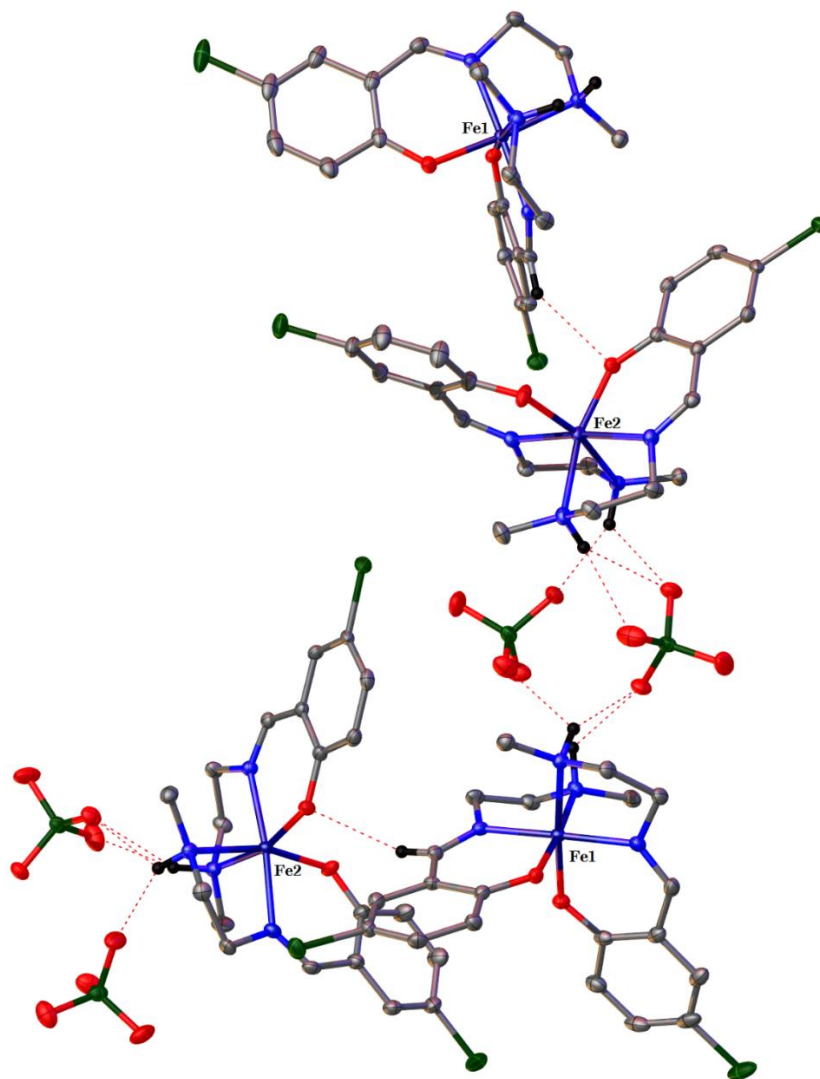


Figure 3. A portion of a chain of hydrogen-bonded complex cations and counter anions in $[\text{Fe}^{\text{III}}(5\text{-Cl-salMeen})_2]\text{ClO}_4$ at 90 K.

The uninegative tridentate Schiff-base ligands in $[\text{Fe}^{\text{III}}(5\text{-X-salMeen})_2]^+$ are arranged very nearly orthogonally relative to each other and the phenolate oxygen, imine nitrogen and amine nitrogen donor atoms adopt the meridional coordination mode. In the distorted octahedral geometry at the iron(III) centre the imine nitrogen atoms take *trans* positions whereas the other pairs of donor atoms of each kind occupy adjacent positions. Selected geometric and distortion parameters for the coordination spheres of compounds **1–4** are presented in Table 4. Within the $[\text{Fe}^{\text{III}}(\text{X-salRen})_2]^+$ system the literature values of the distances for the bonds $\text{Fe}^{\text{III}}\text{-O}_{\text{ph}}$, $\text{Fe}^{\text{III}}\text{-N}_{\text{im}}$ and $\text{Fe}^{\text{III}}\text{-N}_{\text{am}}$ in the HS

state lie in the ranges 1.90–1.96, 2.06–2.14 and 2.17–2.25 Å, respectively, whereas the corresponding ones in the LS state are in the ranges 1.86–1.89, 1.91–1.94 and 2.02–2.06 Å, respectively.^[2-4,26,27,29,31-33,42,43,48] Evidently, both complex cations of compounds **1–4** exist in the HS state at room temperature; however, at 90 K one complex cation is HS whereas the other is LS (Table 4). For the LT structures of compounds **1–4**, the values of $\Delta d_{\text{ave}}(\text{Fe}^{\text{III}}-\text{O})_{\text{HS-LS}}$ are 0.049, 0.049, 0.050 and 0.049 Å, respectively, whereas those of $\Delta d_{\text{ave}}(\text{Fe}^{\text{III}}-\text{N})_{\text{HS-LS}}$ are 0.159, 0.167, 0.158 and 0.157 Å, respectively, confirming that one of the two paramagnetic centres converted to the LS state while the other retained its HS state.^[12,13,26,34a]

The values of the distortion parameter of the *cis* angles, denoted Σ , for the HS and LS complex cations in compounds **1–4** at 90 K fall in the ranges 68.8–72.9° and 52.7–55.2°, respectively (Table 4). The LT and RT values for the HS complex cations are comparable. Furthermore, the HS and LS values of Σ for compounds **1–4** are similar to those observed in other $[\text{Fe}^{\text{III}}(\text{X-salRen})_2]^+$ complex cations.^[2-4,26,29,48] It is noteworthy that for a bis-chelate octahedral iron(III) complex possessing a tridentate Schiff-base ligand derived from *N*-alkylethylenediamine, the HS and LS states are reliably distinguishable by the size of the imine-Fe-amine chelate angle ($\theta_{\text{im-am}}: \text{N}_{\text{im}}-\text{Fe}^{\text{III}}-\text{N}_{\text{am}}$).^[45] Literature values of $\theta_{\text{im-am}}$ for the HS and LS complexes^[2-4,26,27,29,31-33,42,43,48] occur in the ranges ~77–80° and ~83–85°, respectively, which concur with those observed in the series $[\text{Fe}^{\text{III}}(5\text{-X-salMeen})_2]\text{ClO}_4$ (**1–4**) (Table 4). To the best of our knowledge, this is the first crystallographic characterization of spin crossover of the type [HS-HS] \leftrightarrow [HS-LS] within the $[\text{Fe}^{\text{III}}(5\text{-X-salRen})_2]\text{Y}$ family.

Noncovalent intermolecular interactions which are crucial for spin-crossover cooperativity are readily identifiable in the X-ray structures of the series **1–4** (Figures 2–5, S3 and S4, Tables S1–S4). The two complex cations in the asymmetric unit are connected by two perchlorate counter ions through multiple H-bonding interactions ($\text{N}-\text{H}_{\text{amine}}\cdots\text{O}_{\text{perchlorate}}$): each of the secondary amine N–H donors interacts with the perchlorate ions with bifurcated H-bonds. The H-bonds differ in strength within the same complex (LS vs. HS) and across the series **1–4** (Tables S1–S4); they are the strongest of the intermolecular forces present in these compounds, and possibly play a key role in the nature of the spin-transition profiles. Crystal packing reveals dimers of complex cations,¹⁹ formed by $\text{C}-\text{H}_{\text{imine}}\cdots\text{O}_{\text{phenolate}}$ interactions (Figures 2–5 and S2), promoting cooperativity between the paramagnetic centres. Further cooperativity between the complex cations $[\text{Fe}^{\text{III}}(5\text{-X-salMeen})_2]^+$ derives from type-II halogen-halogen bonding interactions,^[36–41] previously not reported for any member of the $[\text{Fe}^{\text{III}}(\text{X-salRen})_2]^+$ family (Figures 4 and S4). These are most dominant in $[\text{Fe}^{\text{III}}(5\text{-I-$

salMeen)₂]ClO₄, but nonexistent in [Fe^{III}(5-F-salMeen)₂]ClO₄, as expected. In the case of [Fe^{III}(5-Cl-salMeen)₂]ClO₄, Cl⋯Cl contacts are observed only at low temperature. Pertinent angles ($\theta_1 = C_1-X_1\cdots X_2$ and $\theta_2 = X_1\cdots X_2-C_2$) and $X_1\cdots X_2$ contacts (92–95% of the sum of van der Waals radii) are shown in Table 3. The I⋯I contacts shown in Figure 4 for [Fe^{III}(5-I-salMeen)₂]ClO₄ exemplify the halogen-halogen bonds in this system. [Fe^{III}(5-F-salMeen)₂]ClO₄ differs also from the other members of this series in that it has a C–H⋯F hydrogen-bonding interaction, which contributes to stabilization of the dimers (Figure 4).

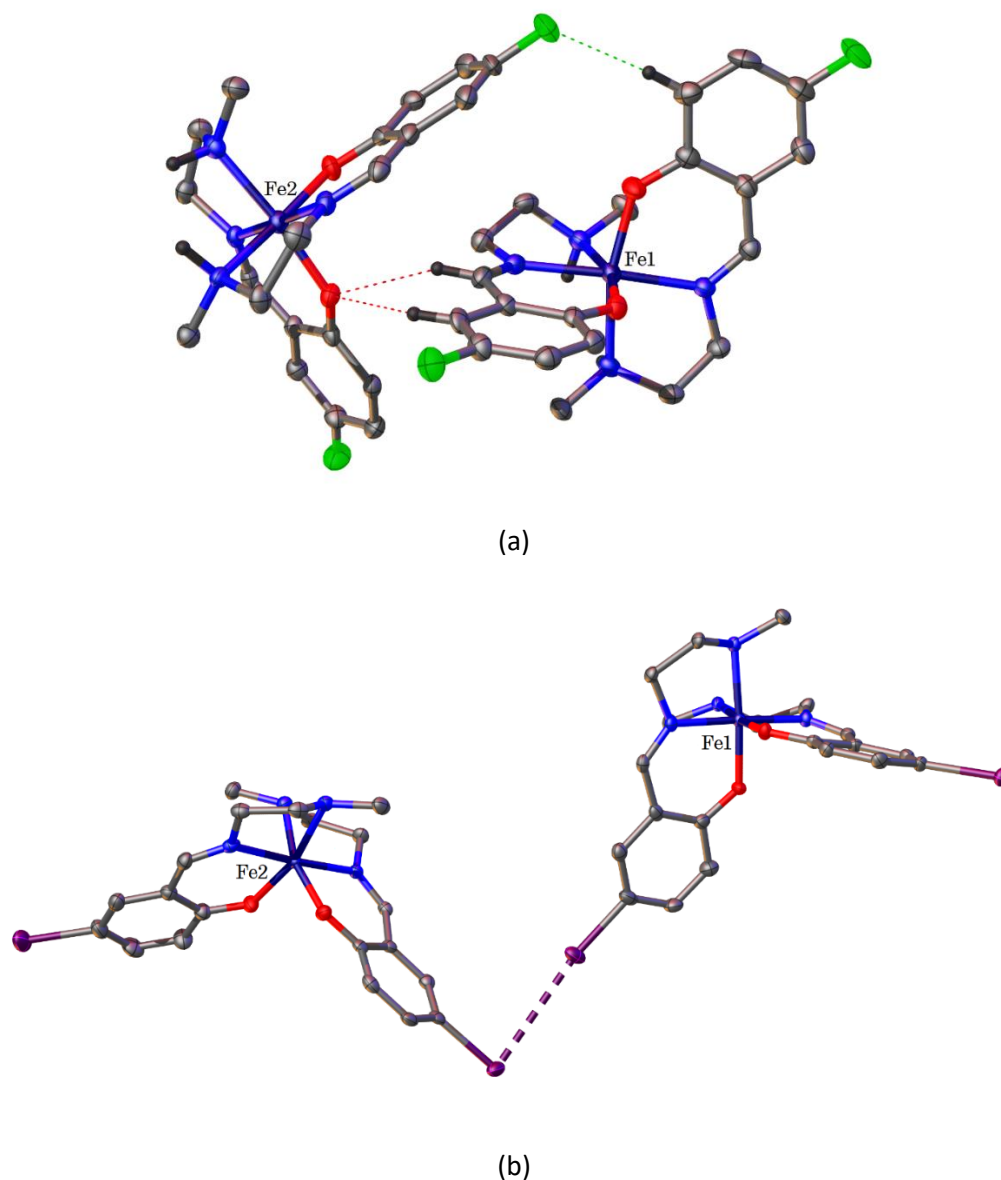
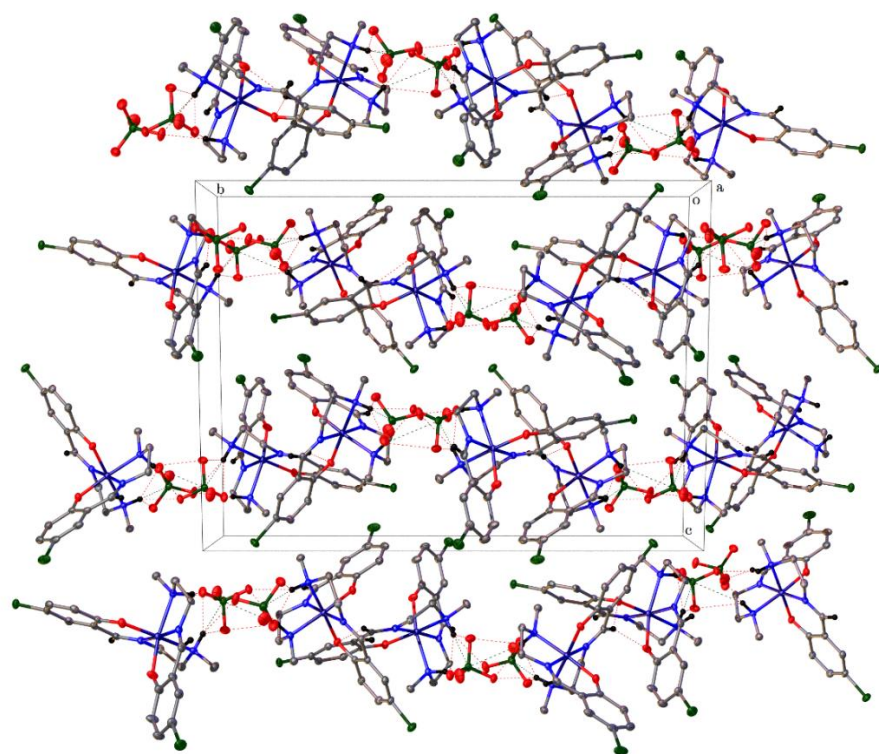


Figure 4. (a) Dimerization in [Fe^{III}(5-F-salMeen)₂]ClO₄ and (b) halogen-halogen bonding interaction in [Fe^{III}(5-I-salMeen)₂]ClO₄ at 90 K.

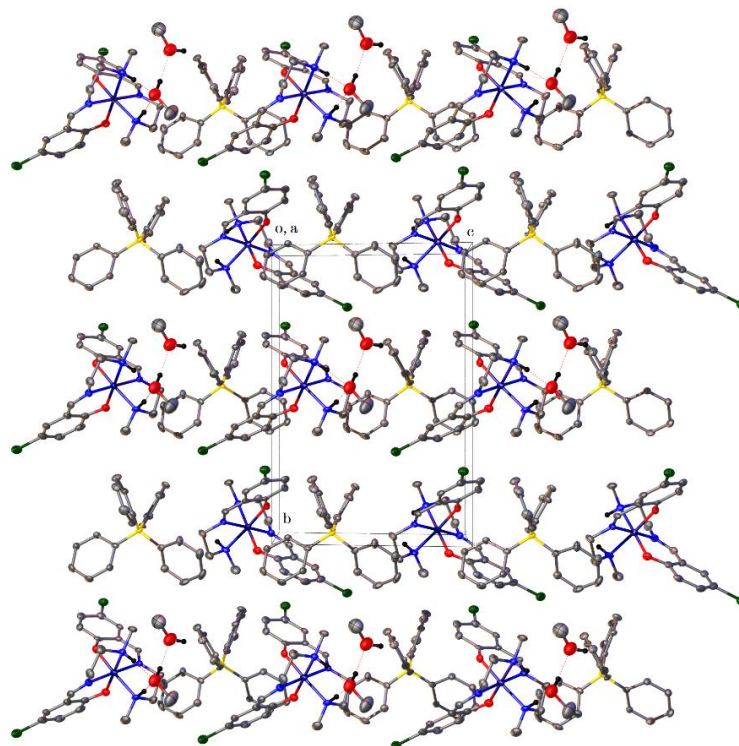
That noncovalent intermolecular forces influence spin-transition profiles is demonstrated spectacularly by the closely related complexes $[\text{Fe}^{\text{III}}(5\text{-Br-salMeen})_2]\text{ClO}_4$ (**3**) and $[\text{Fe}^{\text{III}}(5\text{-Br-salEen})_2]\text{ClO}_4$ (the polymorph designated **1a**, which undergoes complete and abrupt SCO).⁴ Although the ligand anions differ merely by the secondary amine alkyl groups (Me and Et), the magneto-structural properties of complexes **3** and **1a** are markedly different. The major structural differences at LT are summarized as follows: (a) the crystallographic asymmetric unit of **3** consists of two complex cations and two perchlorate counter ions packing in the space group $P2_1/n$ whereas that of **1a** comprises one complex cation and one perchlorate counter ion packing in the space group $P2_1/c$; (b) **3** has a $\text{C-H}_{\text{imine}}\cdots\text{O}_{\text{phenolate}}$ interaction forming dimers of the complex cations, which is not replicated in **1a**; (c) in **3**, two perchlorate counter ions connect two complex cations in the chains, each of the N-H donors interacting with the two perchlorate ions using bifurcated H-bonds, as opposed to the bifurcated single cation-single anion H-bonding in **1a**; (d) the $\text{Fe}\cdots\text{Cl}$ (perchlorate) distance in **1a** (4.919 Å) is shorter than those in **3** ($\text{Fe1}\cdots\text{Cl} = 5.284, 5.297$ Å and $\text{Fe2}\cdots\text{Cl} = 5.130, 5.215$ Å); (e) whereas **3** exhibits Br \cdots Br type II X-bonding (Table 3, Figure S4), **1a** consists of C-Br $\cdots\pi$ interactions and Br \cdots Br type I X-bonding [$\text{Br2}\cdots\text{Br2} = 3.5741(7)$ Å; $\theta_1 = \theta_2 = 145.58(6)^\circ$, Figure S4].

*X-ray structure of $[\text{Fe}^{\text{III}}(5\text{-Cl-salMeen})_2]\text{BPh}_4\cdot 2\text{MeOH}$ (**5·2MeOH**)*

The crystal structure of $[\text{Fe}^{\text{III}}(5\text{-Cl-salMeen})_2]\text{BPh}_4\cdot 2\text{MeOH}$ (**5·2MeOH**) was determined at 298 and 90 K on the same crystal. Selected crystallographic data for **5·2MeOH** are presented in Table 2. Surprisingly, this iron(III) compound undergoes a temperature-dependent crystallographic phase transition from orthorhombic $C222_1$ at RT to monoclinic $P2_1$ at LT with retention of the spin state. The LT packing diagrams of $[\text{Fe}^{\text{III}}(5\text{-Cl-salMeen})_2]\text{ClO}_4$ and $[\text{Fe}^{\text{III}}(5\text{-Cl-salMeen})_2]\text{BPh}_4\cdot 2\text{MeOH}$ having the same orientation contrast sharply (Figure 5). In the latter compound, the larger BPh_4^- ions alternate, but do not interact, with the complex cations; in the former the smaller ClO_4^- ions allow close packing of the dimers of the complex cations and promote formation of chains of the dimers through H-bonding. Given that these entities occupy similar positions at both temperatures, the most likely cause of the phase transition in **5·2MeOH** is the greater thermal motion of the solvent molecules at room temperature. Whereas in the structure of $[\text{Fe}^{\text{III}}(5\text{-Cl-salMeen})_2]\text{ClO}_4$ (**2**) the two secondary amine groups are hydrogen-bonded to two ClO_4^- ions, in the structure of $[\text{Fe}^{\text{III}}(5\text{-Cl-salMeen})_2]\text{BPh}_4\cdot 2\text{MeOH}$ (**5·2MeOH**) these aforementioned ligand functional groups are hydrogen-bonded to one MeOH molecule which in turn is hydrogen-bonded to the other MeOH molecule.



(a)



(b)

Figure 5. Crystal packing diagrams for (a) $[\text{Fe}^{\text{III}}(5\text{-Cl-salMeen})_2]\text{ClO}_4$ and (b) $[\text{Fe}^{\text{III}}(5\text{-Cl-salMeen})_2]\text{BPh}_4 \cdot 2\text{MeOH}$

As observed in $[\text{Fe}^{\text{III}}(5\text{-Cl-salMeen})_2]\text{ClO}_4$, the orientation of the two uninegative tridentate Schiff-base ligands in $[\text{Fe}^{\text{III}}(5\text{-Cl-salMeen})_2]\text{BPh}_4 \cdot 2\text{MeOH}$ relative to each other is very nearly orthogonal and the donor atoms adopt the meridional coordination arrangement. The 3-D structures of the complex cation $[\text{Fe}^{\text{III}}(5\text{-Cl-salMeen})_2]^+$ in $[\text{Fe}^{\text{III}}(5\text{-Cl-salMeen})_2]\text{BPh}_4 \cdot 2\text{MeOH}$ at 298 and 90 K differ in that that at the higher temperature exhibits C_2 -symmetry with the distances of the bonds $\text{Fe}^{\text{III}}\text{-O}_{\text{ph}}$, $\text{Fe}^{\text{III}}\text{-N}_{\text{im}}$ and $\text{Fe}^{\text{III}}\text{-N}_{\text{am}}$ being 1.852, 1.921 and 2.037 Å, respectively. For the structure at the lower temperature, the average distances for the corresponding bonds are 1.865, 1.928 and 2.034 Å, respectively. The values of Σ and $\theta_{\text{im-am}}$ (39.9° and 83.7° , respectively) for the RT structure are very similar to those of the LT structure (41.7° and $83.7/83.4^\circ$, respectively). These $\text{Fe}^{\text{III}}\text{-L}$ distances and octahedral distortion parameters (Table 5) point to the LS state of the complex cations at both temperatures.

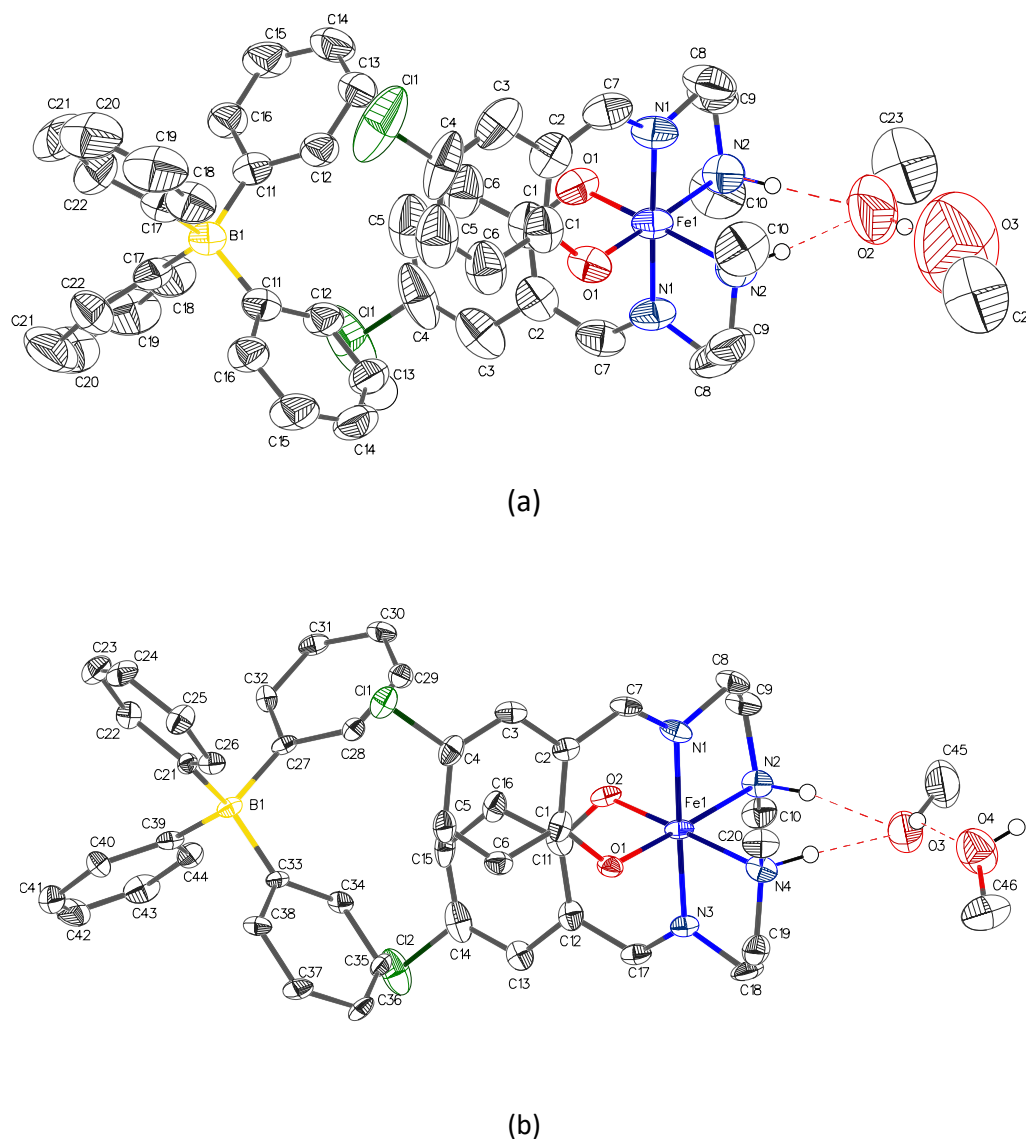


Figure 6. X-ray structure of $[\text{Fe}^{\text{III}}(5\text{-Cl-salMeen})_2]\text{BPh}_4 \cdot 2\text{MeOH}$ at (a) 300 K and (b) 90 K.

Magnetic Susceptibility Measurements and Mössbauer Spectroscopy

Spin-transition profile for $[\text{Fe}^{\text{III}}(5\text{-X-salMeen})_2]\text{ClO}_4$ ($X = \text{F}, \text{Cl}, \text{Br}, \text{I}$) (**1–4**)

Variable-temperature SQUID measurements were carried out principally to determine the spin-transition profile for the [HS-HS] \rightarrow [HS-LS] conversion deduced from the single-crystal X-ray analyses of complexes **1–4**. Plots of $\chi_{\text{M}}T$ versus absolute temperature (5–300 K) are presented in Figure 7. The room-temperature values of $\chi_{\text{M}}T$ for **1–4**, which occur in the range 4.06–4.28 $\text{cm}^3 \text{K mol}^{-1}$, are consistent with the spin-only value for HS iron(III) ($\chi_{\text{M}}T \sim 4.38 \text{ cm}^3 \text{K mol}^{-1}$). They also concur with literature values in the range 3.80–4.50 $\text{cm}^3 \text{K mol}^{-1}$ for closely related ferric spin-crossover materials,^[1-20,24,29,34,35,45,46,48-51] although some of these reported values are somewhat low.^[12,14-16,49] The spin conversion in **1–4**, evidenced by the decrease in the values of $\chi_{\text{M}}T$ with temperature, culminates in a plateau with a width of 115 K (140–25 K) for **2–4** and 85 K (110–25 K) for **1**. The sharp drop of the values of $\chi_{\text{M}}T$ below 25 K is attributable to the zero-field splitting of the ${}^6\text{A}_1$ ground state for the complex cations trapped in the HS state. The magnetic plateau is characterized by $\chi_{\text{M}}T$ values between 2.25 and 2.53 $\text{cm}^3 \text{K mol}^{-1}$ indicative of the coexistence of HS and LS populations in equal proportions, in accord with the crystallographic analyses of **1–4** at 90 K. This spin-transition profile featuring a [HS-LS] plateau is rare in the $[\text{Fe}^{\text{III}}(\text{R}^1\text{-salRen})_2]\text{Y}$ family and is reminiscent of that exhibited by $[\text{Fe}^{\text{III}}(4\text{-OMe-salMeen})_2]\text{PF}_6$ ^[24] and the closely related saltrien complexes $[\text{Fe}^{\text{III}}]\text{PF}_6$ ($\text{H}_2\text{L} = \text{H}_2\text{-5-}^i\text{Pr-saltrien}$ or $\text{H}_2\text{-5-}^t\text{Bu-saltrien}$),^[52] which unfortunately were not crystallographically elucidated.

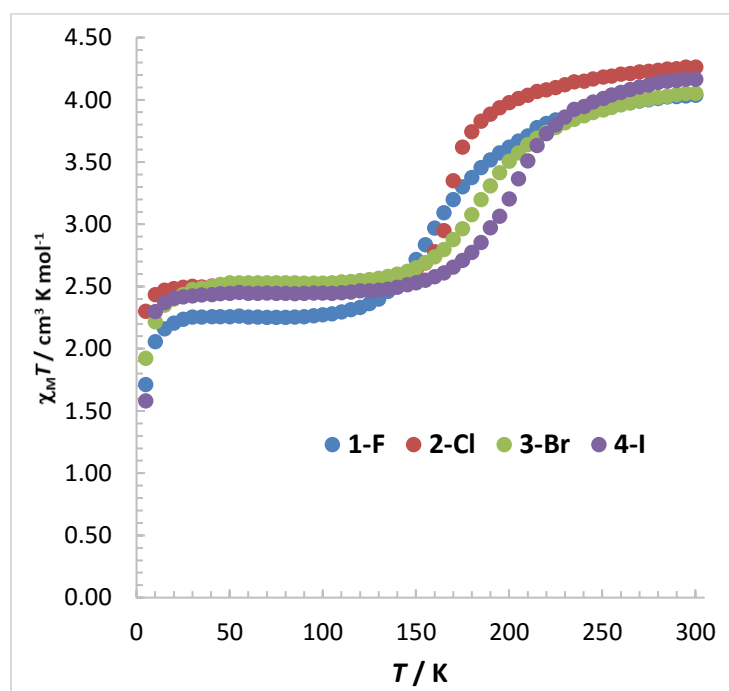


Figure 7. Temperature dependence of effective magnetic moment for $[\text{Fe}^{\text{III}}(5\text{-X-salMeen})_2]\text{ClO}_4$ (**1–4**)

Of the compounds **1–4**, $[\text{Fe}^{\text{III}}(\text{5-Cl-salMeen})_2]\text{ClO}_4$ (**2**) undergoes the steepest spin transition; on the other hand, the spin conversion is most gradual for $[\text{Fe}^{\text{III}}(\text{5-F-salMeen})_2]\text{ClO}_4$ (**1**). The plots of $\chi_{\text{M}}T$ vs. T for **1–4** give the approximate $T_{1/2}$ values 160, 168, 180 and 195 K, respectively. For $[\text{Fe}^{\text{III}}(\text{5-Cl-salMeen})_2]\text{ClO}_4$ (**2**), magnetic data were collected during cooling and warming of the sample in order to investigate any hysteretic behaviour. Indeed, this compound does exhibit SCO hysteresis though modest (Figure 8); the hysteresis loop cannot be determined with much certainty given the high scan rate (5 K/min) and large temperature interval for the magnetic susceptibility measurements. Although the overall structures of the compounds $[\text{Fe}^{\text{III}}(\text{5-X-salMeen})_2]\text{ClO}_4$ are similar there are subtle differences in the noncovalent intermolecular forces which might account for the slight differences in the magnetic profiles, the most significant of which are the H-bonding interactions between the complex cations and the perchlorate counter ions (Tables S1–S4). There are also differences in the halogen-halogen bonding interactions ($\text{C}_1\text{--X}_1\cdots\text{X}_2\text{--C}_2$) [Table 3, Figures 5(b) & 4S], which are most dominant in the structures of $[\text{Fe}^{\text{III}}(\text{5-Br-salMeen})_2]\text{ClO}_4$ and $[\text{Fe}^{\text{III}}(\text{5-I-salMeen})_2]\text{ClO}_4$. While $[\text{Fe}^{\text{III}}(\text{5-F-salMeen})_2]\text{ClO}_4$ does not exhibit such interactions, it does have a weak C–H \cdots F hydrogen-bonding interaction between the HS and LS complex cations [Figure 5(a)] at 100 K, the type of which none of the other members of this series possess.

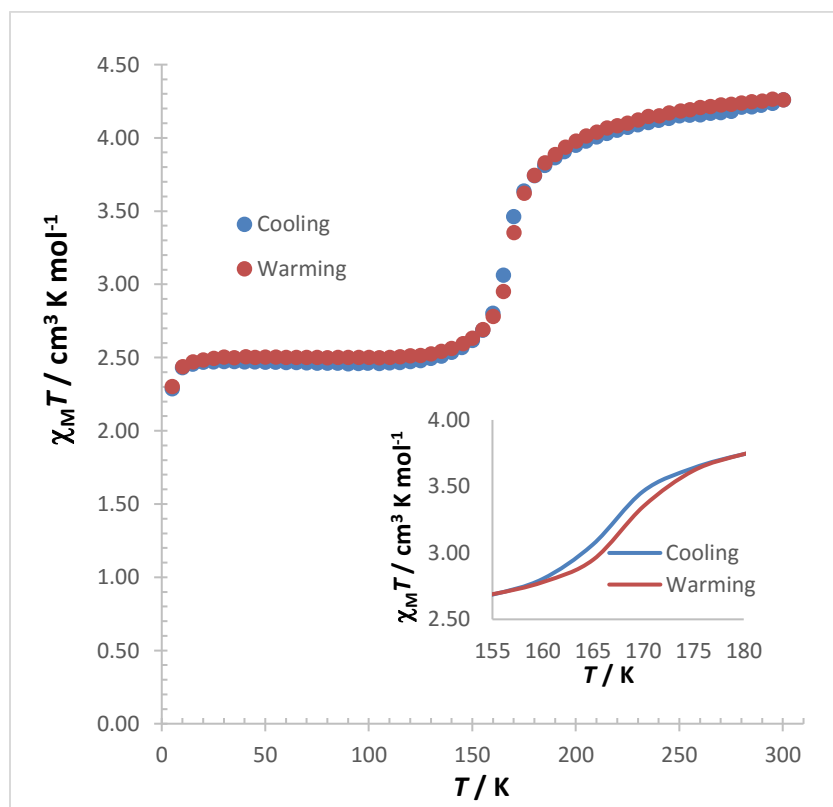
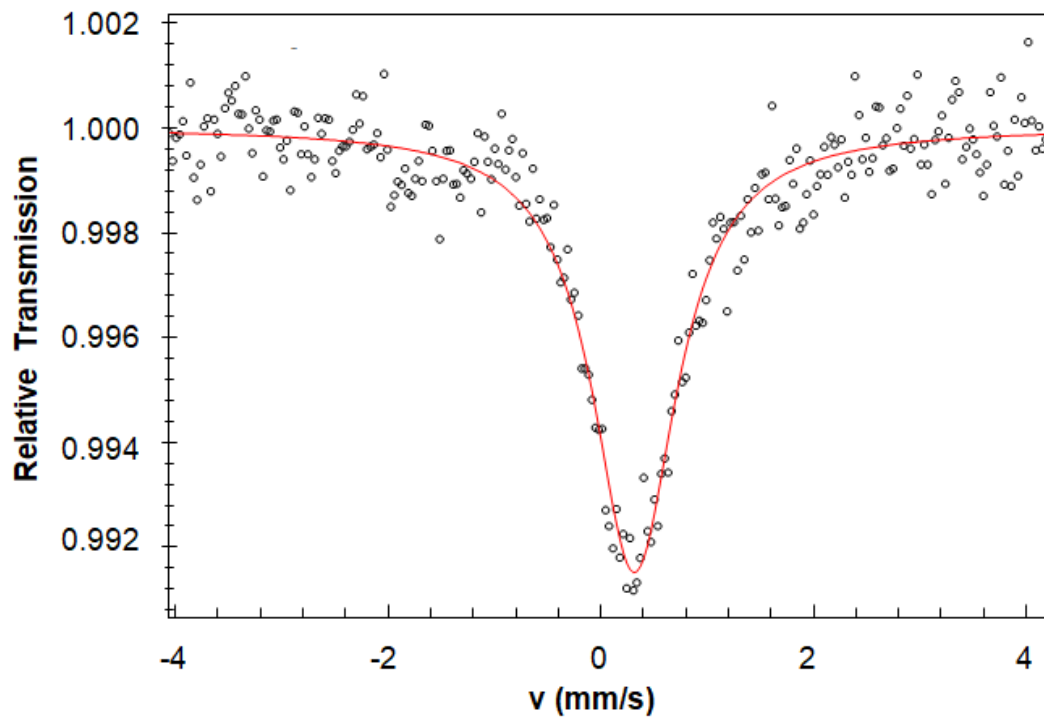


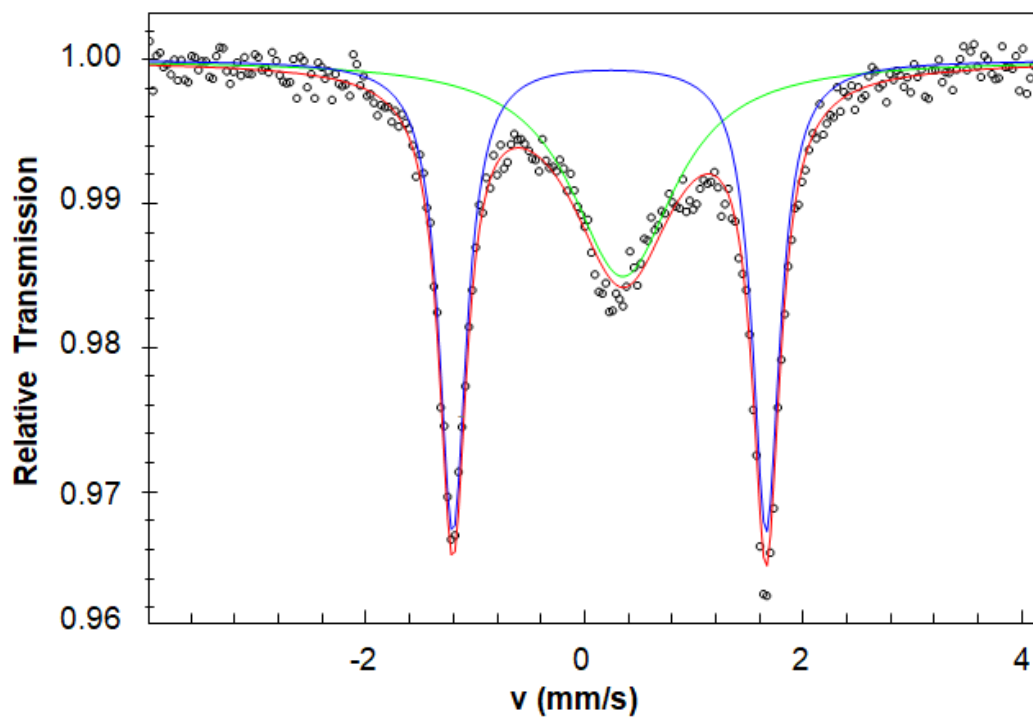
Figure 8. Hysteretic behaviour of $[\text{Fe}^{\text{III}}(\text{5-Cl-salMeen})_2]\text{ClO}_4$.

The ^{57}Fe Mössbauer effect has proven to be an invaluable spectroscopic tool to investigate ferric spin crossover occurring in pure solid materials. For slow ${}^6\text{A}_1 \leftrightarrow {}^2\text{T}_2$ interconversions ($< 10^7 \text{ s}^{-1}$) on the ^{57}Fe Mössbauer time scale ($\sim 10^{-7} \text{ s}$), distinct HS and LS resonances are observable in the Mössbauer spectrum.^[1b,25,27,28,53] The Mössbauer spectra of $[\text{Fe}^{\text{III}}(5\text{-I-salMeen})_2]\text{ClO}_4$ (**4**) recorded at room temperature ($\chi_{\text{MT}} = 4.21 \text{ cm}^3 \text{ K mol}^{-1}$) and at 80 K ($\chi_{\text{MT}} = 2.45 \text{ cm}^3 \text{ K mol}^{-1}$) are displayed in Figure 9. The broad absorption peak^[4,14,16,17,29,54] in the RT spectrum with an isomer shift (δ) of 0.32 mm s^{-1} (relative to $\alpha\text{-Fe}$) is characteristic of HS iron(III), although in some HS iron(III) complexes a narrow doublet^[9,12,15] or a broad asymmetric doublet^[5,19,20,34a] is observed instead. To double-check the purity of the nondegenerate ground state of the complexes in this series at RT, the Mössbauer spectrum of $[\text{Fe}^{\text{III}}(5\text{-Cl-salMeen})_2]\text{ClO}_4$ (**2**) was also recorded, likewise giving a broad symmetrical resonance ($\delta = 0.26 \text{ mm s}^{-1}$) (Figure S2). Given the quenching of the orbital contribution to paramagnetism in HS Fe^{III} complexes ($S = 5/2$, $L = 0$), the broadening of the Mössbauer signal for HS Fe^{III} is most likely related to spin-spin relaxation^[16-18,55] on the Mössbauer time scale. On cooling the sample of $[\text{Fe}^{\text{III}}(5\text{-I-salMeen})_2]\text{ClO}_4$ (**4**) to liquid-nitrogen temperature, the Mössbauer spectrum reveals a wide LS (${}^2\text{T}_2$) quadrupole-split doublet ($\delta = 0.23 \text{ mm s}^{-1}$ and $\Delta E_{\text{Q}} = 2.87 \text{ mm s}^{-1}$) in addition to the broad HS (${}^6\text{A}_1$) signal with $\delta = 0.35 \text{ mm s}^{-1}$.

According to the plot of χ_{MT} vs. T , the [HS-LS] plateau temperatures lie in the range 30–145 K, where the HS and LS complex cations exist in equal proportions. The relative intensities of the HS and LS Mössbauer absorptions (I_{HS} and I_{LS}) at 80 K imply that the amounts of the HS and LS species are in the ratio of 45 : 55. Minor discrepancies between magnetic susceptibility data and Mössbauer spectra are quite common;^[16,30] in the case of the series $[\text{Fe}^{\text{III}}(\text{X-salEen})_2]\text{Y}$, Hendrickson *et al.*^[1b] provided an explanation in terms of the Debye-Waller factor which determines the recoilless fraction for HS and LS species. As always observed crystallographically, the $\text{Fe}^{\text{III}}\text{-L}$ bonds for the LS state are significantly shorter and stronger than the corresponding HS ones, causing a larger recoilless fraction for the LS complex cations. In addition, for the $[\text{Fe}^{\text{III}}(\text{X-salEen})_2]\text{Y}$ compounds, it was established from systematic studies that sample grinding shifts the interconversion $S = 5/2 \leftrightarrow S = 1/2$ in favour of the low-spin state.^[25] In the case of $[\text{Fe}^{\text{III}}(5\text{-I-salMeen})_2]\text{ClO}_4$ (**4**), the sample for the magnetic susceptibility measurements was microcrystalline whereas that for the Mössbauer measurements was a finely ground powder.



(a)



(b)

Figure 9. Mössbauer spectra of $[\text{Fe}(\text{5-I-salMeen})_2]\text{ClO}_4$ at (a) 293 K and (b) 80 K.

Magnetic profile for [Fe^{III}(5-Cl-salMeen)₂]BPh₄·2MeOH (5·2MeOH)

The magnetic curve for [Fe^{III}(5-Cl-salMeen)₂]BPh₄·2MeOH is shown in Figure 10(a). The crystallographic metric parameters for the coordination geometry of this compound point to the low-spin state. Generally, close to liquid-helium temperature the values of $\chi_{\text{M}}T$ are commonly observed in the range 0.45–0.50 cm³ K mol⁻¹ whereas at room temperature they can be as high as 0.83 cm³ K mol⁻¹.^[24,26,55] For 5·2MeOH, the values of $\chi_{\text{M}}T$ (0.48–0.85 cm³ K mol⁻¹) suggest the onset of a spin transition above 220 K. Similar magnetic behaviour was observed for [Fe^{III}(3-OMe-salMeen)₂]PF₆^[24,26] whereby the values of $\chi_{\text{M}}T$ rose from 0.67 cm³ K mol⁻¹ at 78 K to 1.22 cm³ K mol⁻¹ at 298 K, and this compound was estimated to be ~ 70% LS at room temperature. However, crystallographic analysis revealed a discrepancy in that the octahedral angular distortion parameters and Fe^{III}–L bond distances were consistent with 100% LS state. Considering the presence of voids in the crystal lattice of 5·2MeOH into which the solvent molecules can move and the greater thermal motions of the solvents at higher temperatures, the magnetic properties of this compound are susceptible to change on sample grinding.^[25,34a,52] Indeed the Mössbauer spectrum of 5·2MeOH recorded at 300 K shows the presence of both the LS ($\delta = 0.15$ mm/s, $\Delta E_{\text{Q}} = 2.66$ mm/s) and HS ($\delta = 0.27$ mm/s, $\Delta E_{\text{Q}} = 0.56$ mm/s) states^{34a} in a ratio of ~ 80 : 20% [Figure 10(b)].

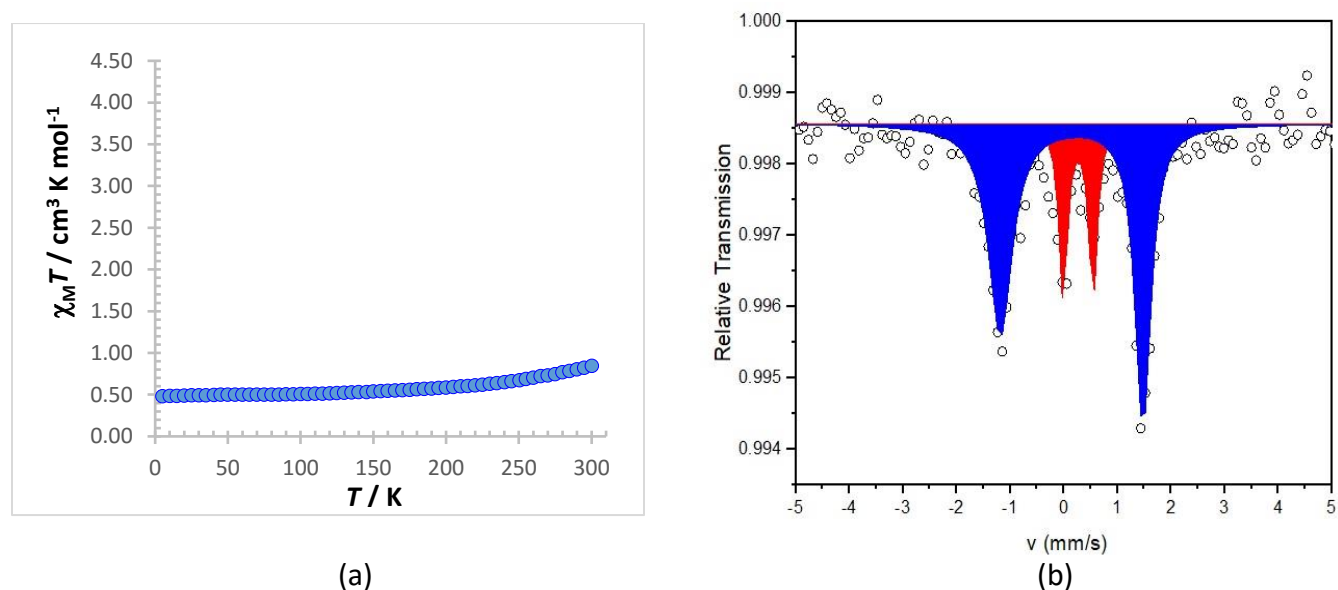


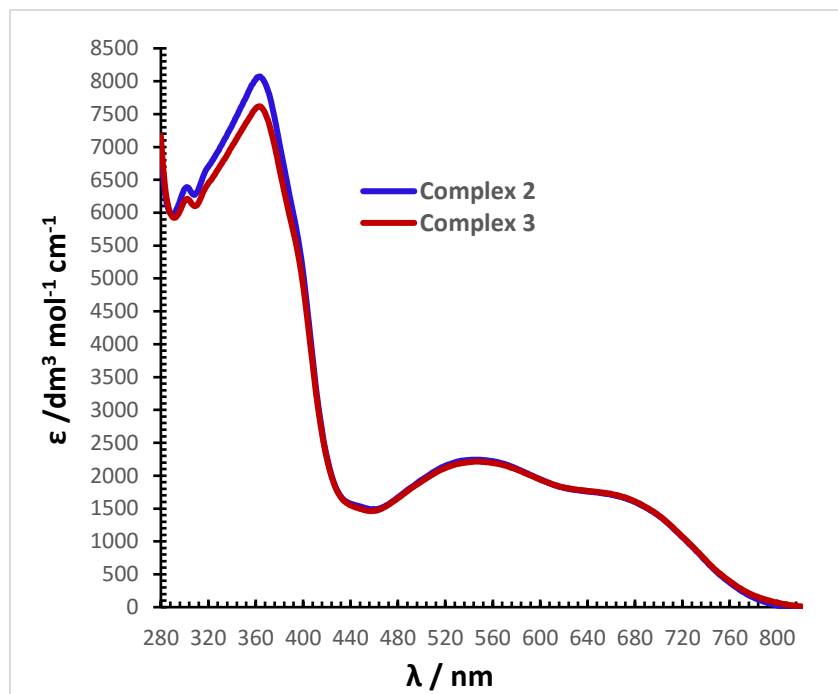
Figure 10. Plot of $\chi_{\text{M}}T$ vs. T for 5·2MeOH (a) and Mössbauer spectrum of 5·2MeOH at 300 K (b).

Solution Spin-State Equilibria

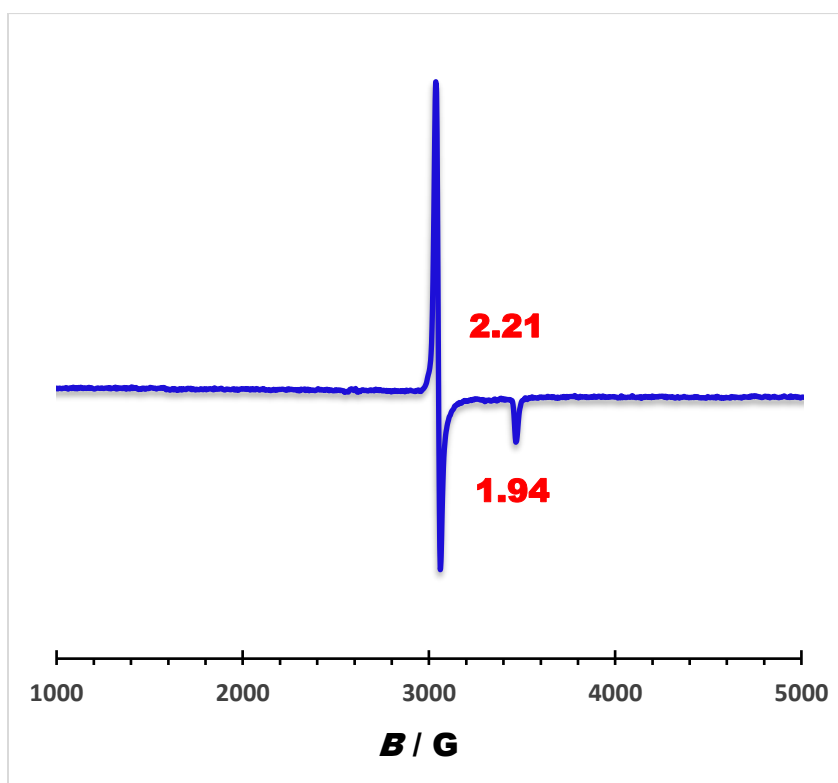
The interconversions between the HS and LS states in the series $[\text{Fe}^{\text{III}}(5\text{-X-salMeen})_2]\text{ClO}_4$ (**1–4**) in solution were investigated by visible and EPR spectroscopic techniques using methanol as a solvent. Electronic spectroscopy reveals an overlap of HS and LS absorption spectra for each complex at room temperature. The LMCT absorptions occur around 360 nm and in the region 460–800 nm. The charge-transfer spectra for $[\text{Fe}^{\text{III}}(5\text{-Cl-salMeen})_2]\text{ClO}_4$ (**2**) and $[\text{Fe}^{\text{III}}(5\text{-Br-salMeen})_2]\text{ClO}_4$ (**3**), depicted in Figure 11(a), demonstrate a remarkable correlation between the electronic spectra and the Hammett parameters (σ_p , Table 6).^[56] The UV LMCT bands ($\lambda \sim 363$ nm) are attributable to phenolate (p_π) \rightarrow iron(III) (d_{σ^*}) electronic transitions whereas the broad lopsided visible LMCT bands are phenolate (p_π) \rightarrow iron(III) (d_π) in nature.^[34a,45,46,50,51,57-59]

The HS and LS states of the complexes $[\text{Fe}^{\text{III}}(5\text{-X-salMeen})_2]\text{ClO}_4$ (**1–4**) in electronic spectroscopy are distinguishable by their visible charge-transfer absorptions.^[24,45] Given that $\Delta_o < P$ for the HS state and $\Delta_o > P$ for the LS state, there is greater stabilization of the Fe^{III} d_π orbitals in the LS state than in the HS state. Consequently, the energy separation between the phenolate p_π and the Fe^{III} d_π orbitals is smaller in the LS complex cations, causing the LS visible charge-transfer absorptions to occur at longer wavelengths. For complexes **2** and **3** [Figure 11(a)], the HS and LS charge-transfer absorptions are centred at 546 nm ($\epsilon_{\text{max}} \sim 2240 \text{ dm}^3 \text{ mol}^{-1} \text{ cm}^{-1}$) and 680 nm ($\epsilon_{\text{max}} \sim 1600 \text{ dm}^3 \text{ mol}^{-1} \text{ cm}^{-1}$), comparable to those reported for the closely related complex $[\text{Fe}^{\text{III}}(\text{salMeen})_2]\text{PF}_6$.^[24] The existence of both spin states in methanol solution at room temperature is in sharp contrast to the magnetic data of the pure solids at the same temperature.

X-band EPR spectroscopy revealed that all the complexes $[\text{Fe}^{\text{III}}(5\text{-X-salMeen})_2]\text{ClO}_4$ (**1–4**) are fully LS in frozen methanol solution at liquid-nitrogen temperature and their EPR spectra are virtually indistinguishable from one another (see Experimental Section in Supporting Information). LS Fe^{III} EPR spectra tend to be either rhombic^[28,35,42,49,53,60,62] or axial.^[19,27,49,53,58] Those of complexes **1–4**, represented by the spectrum of $[\text{Fe}^{\text{III}}(5\text{-Cl-salMeen})_2]\text{ClO}_4$ (**2**) [Figure 11(b): $g_\perp = 2.21$ and $g_\parallel = 1.94$], are consistent with the latter. Evidently, the spin-state conversion in the pure solids is different from that in solution. It is plausible that the hydrogen bonds between the complex cations and between the complex cations and perchlorate counter ions in compounds **1–4** break during the dissolution in methanol, and new noncovalent interactions involving the solvent molecules are expected.



(a)



(b)

Figure 11. (a) Charge-transfer spectra of $[\text{Fe}^{\text{III}}(5\text{-Cl-salMeen})_2]\text{ClO}_4$ (blue) and $[\text{Fe}^{\text{III}}(5\text{-Br-salMeen})_2]\text{ClO}_4$ (red) in MeOH and (b) X-band EPR spectrum of a frozen MeOH solution of $[\text{Fe}^{\text{III}}(5\text{-Cl-salMeen})_2]\text{ClO}_4$ at 80 K.

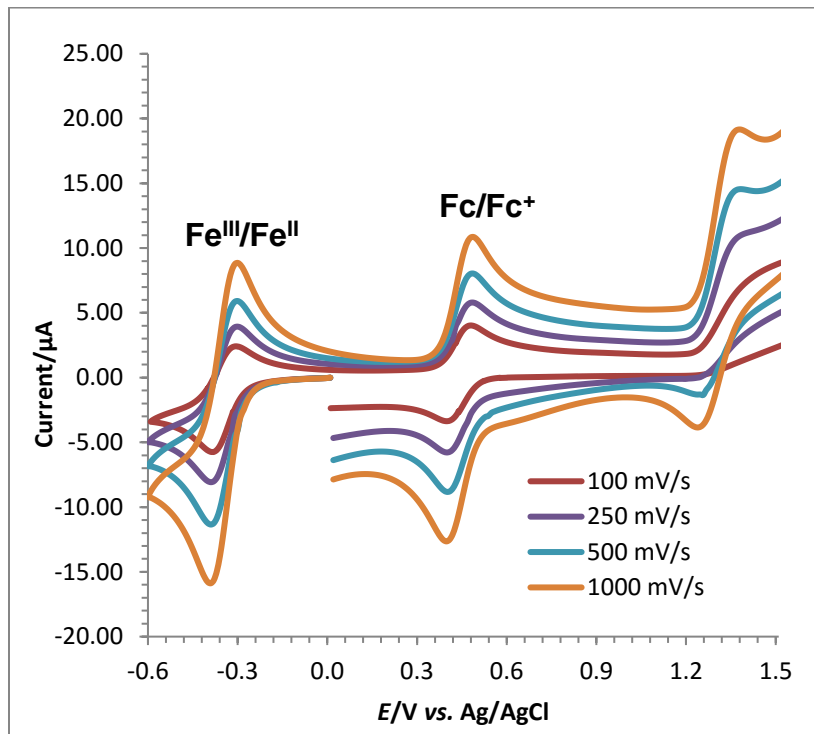
Electrochemical Processes

The redox chemistry of the compounds $[\text{Fe}^{\text{III}}(5\text{-X-salMeen})_2]\text{ClO}_4$ (**1–4**) was explored with the aid of cyclic voltammetry. Given the stabilization of the divalent state of iron in the spin-crossover complexes $[\text{Fe}^{\text{II}}(3\text{-X},5\text{-NO}_2\text{-sal-N}(1,4,7,10))]$ ($\text{X} = \text{H}, \text{OMe}, \text{OEt}$)^[63] by the $[\text{N}_4\text{O}_2]^{2+}$ donor set identical to that in $[\text{Fe}^{\text{III}}(5\text{-X-salMeen})_2]\text{ClO}_4$ (**1–4**), a thermodynamically favourable metal-centred one-electron reductive process is expected of the Fe^{III} -salMeen complexes. The cyclic voltammograms of $[\text{Fe}^{\text{III}}(5\text{-X-salMeen})_2]\text{ClO}_4$ ($\text{X} = \text{F}, \text{Cl}, \text{Br}, \text{I}$), including the unsubstituted complex $[\text{Fe}^{\text{III}}(\text{salMeen})_2]\text{ClO}_4$ for comparison, are displayed in Figure 12 and the half-wave potentials ($E_{1/2}$) along with other parameters pertinent to the redox processes are presented in Table 6. The potentials of the compounds (1 mM in CH_3CN) at RT were recorded *versus* Ag/AgCl (reference electrode) under argon with ferrocene as an internal standard (Fc/Fc^+ , $E_{1/2} = 0.440$ V) and $[\text{Bu}_4\text{N}]\text{PF}_6$ as supporting electrolyte.

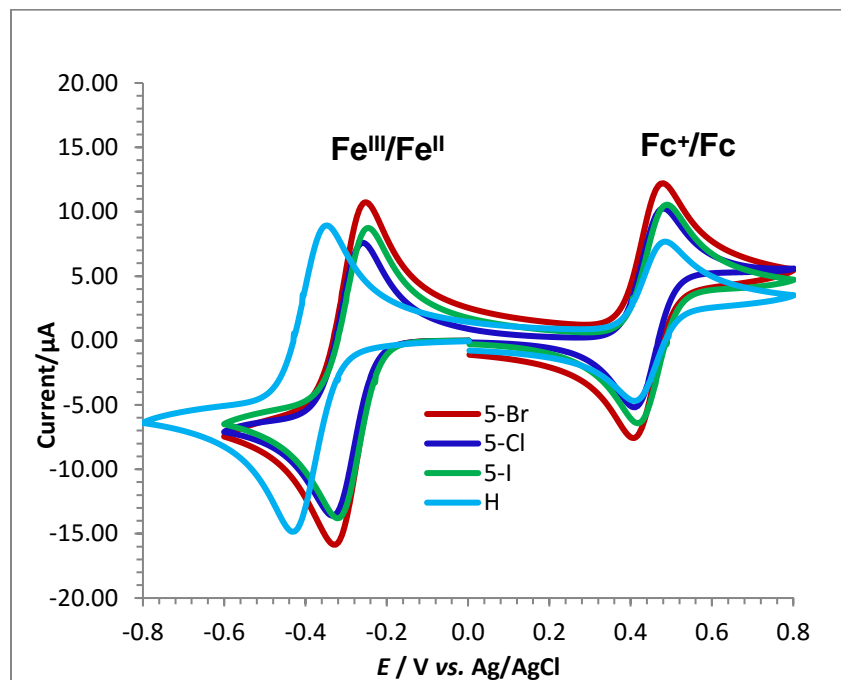
The cyclic voltammograms of $[\text{Fe}^{\text{III}}(5\text{-F-salMeen})_2]\text{ClO}_4$ measured at different scan rates [Figure 12 (a)] show a reversible wave for the $\text{Fe}^{\text{III}}/\text{Fe}^{\text{II}}$ couple at -0.35 V (-0.79 V *vs.* Fc/Fc^+). A ligand-centred redox process at $+1.31$ V ($+0.87$ V *vs.* Fc/Fc^+), whose reversibility increases with the scan rate, is associated with oxidation of the phenolate moiety to a phenoxy radical.^[45,58,64] The cyclic voltammograms of the rest of the members of this series along with the unsubstituted compound $[\text{Fe}^{\text{III}}(\text{salMeen})_2]\text{ClO}_4$ are exhibited in Figure 12 (b). A quantitative measure of the electronic effect of a substituent group is given by a Hammett parameter (σ_p),^[56] which comprises inductive and resonance factors (σ_I and σ_R) with opposing effects. The effects of non-halogen electron-withdrawing and electron-donating substituent groups (e.g. $-\text{NO}_2$ and $-\text{Me}$, respectively) on the acidity of corresponding phenols and the redox potentials of corresponding iron(III)-phenolate complexes are readily predictable and explicable.

Intriguingly, the patterns of the pK_a values of the *para*-halo-substituted phenols and the Hammett parameters in relation to the electronegativity values of the corresponding halogens would seem paradoxical. However, for phenol and *para*fluorophenol, the comparable values of pK_a (9.99 and 9.89, respectively) and σ_p ($\text{H} = 0.00$ and $\text{F} = 0.06$) demonstrate the importance of the contribution of the resonance effect (σ_R) to the overall Hammett constant ($\sigma_p = \sigma_I + \sigma_R$). The electron-withdrawing capacity of the fluoro substituent is greatly diminished by the magnitude of σ_R . Hence the redox potential of $[\text{Fe}^{\text{III}}(5\text{-F-salMeen})_2]\text{ClO}_4$ is comparable with that of the unsubstituted compound $[\text{Fe}^{\text{III}}(\text{salMeen})_2]\text{ClO}_4$. The trend in the redox potentials of the complexes $[\text{Fe}^{\text{III}}(5\text{-X-salMeen})_2]\text{ClO}_4$ (X

= F, Cl, Br, I) is consistent with the Hammett parameters for the respective halogen substituents (Table 6): the more positive the value of σ_p , the more spontaneous the $\text{Fe}^{\text{III}}/\text{Fe}^{\text{II}}$ redox process.



(a)



(b)

Figure 12. Cyclic voltammograms for (a) $[\text{Fe}^{\text{III}}(5\text{-F-salMeen})_2]\text{ClO}_4$ at different scan rates and (b) $[\text{Fe}^{\text{III}}(5\text{-X-salMeen})_2]\text{ClO}_4$ (X = H, Cl, Br, I) at a scan rate of 100 mV/s.

Concluding Remarks

The compounds $[\text{Fe}^{\text{III}}(5\text{-X-salMeen})_2]\text{ClO}_4$ ($\text{X} = \text{F}, \text{Cl}, \text{Br}, \text{I}$) (**1–4**) and $[\text{Fe}^{\text{III}}(5\text{-Cl-salMeen})_2]\text{BPh}_4 \cdot 2\text{MeOH}$ (**5**) have been produced straightforwardly and isolated as black crystals. Their chemical identities have been established by pertinent analytical, spectroscopic and crystallographic techniques. Single-crystal X-ray analyses of compounds **1–4** shows that at room temperature the asymmetric unit consists of a pair of discrete complex cations both of which are in the high-spin state [HS-HS]. However, at 90 K one of the complex cations has converted to the low-spin state, resulting in a mixed spin-state phase [HS-LS]. The packing diagrams at RT and LT reveal chains comprising dimers of complex cations linked via pairs of perchlorate counter ions through H-bonding interactions. Moreover, compounds **2–4** exhibit type-II halogen-halogen bonding interactions. Variable-temperature SQUID measurements revealed a spin-transition profile consistent with half spin crossover having a wide plateau ($\chi_{\text{M}}T$ values: $\sim 2.25\text{--}2.53 \text{ cm}^3 \text{ K mol}^{-1}$). In the case of $[\text{Fe}^{\text{III}}(5\text{-I-salMeen})_2]\text{ClO}_4$ (**4**), this magnetic behaviour was corroborated by Mössbauer spectroscopy. This cooperative [HS-HS] \leftrightarrow [HS-LS] spin transition has not been crystallographically elucidated previously within the $[\text{Fe}^{\text{III}}(\text{X-salRen})_2]\text{Y}$ family. $[\text{Fe}^{\text{III}}(5\text{-Cl-salMeen})_2]\text{BPh}_4 \cdot 2\text{MeOH}$ (**5**·2MeOH) undergoes a temperature-dependent crystallographic phase transition associated with the thermal motions of the solvent molecules while retaining the LS state. However, as a finely ground powder, **5**·2MeOH exhibits $\sim 20\%$ SCO to the HS state. As homogeneous mixtures with methanol, the compounds **1–4** exhibit different magnetic behaviour than as pure solids. EPR spectroscopy showed that the low-spin state in all complexes **1–4** is fully accessible at liquid-nitrogen temperature in frozen methanol solution. Finally, all compounds **1–4** are electroactive and the trend of their metal-centred redox potentials is in keeping with the values of the Hammett parameters for the halogen substituents.

Experimental Section

Materials, Methods and Physicochemical Measurements

Detailed synthetic procedures for the complexes $[\text{Fe}(5\text{-X-salMeen})_2]\text{ClO}_4$ (**1–4**) and $[\text{Fe}(5\text{-X-salMeen})_2]\text{BPh}_4 \cdot 2\text{MeOH}$ (**5**·2MeOH) and data for chemical identification are provided as supporting information. *N*-Methylethylenediamine, *para*-substituted salicylaldehydes, iron(III) perchlorate hydrate as well as reagents and solvents (HPLC/AR-grade) were purchased from Sigma-Aldrich and used as received. **Caution:** salts of perchlorates are notorious for their tendency to explode, hence

their samples must be handled with due care and in small quantities. Microanalyses (CHN) were performed on a EuroEA elemental analyzer and mass spectra were recorded on an Agilent 6460 Triple Quad LC mass spectrometer in both positive and negative modes. $^1\text{H-NMR}$ spectroscopic measurements of selected Schiff bases were carried out in $\text{DMSO-}d_6$ on a Bruker ASCEN 700 MHz NMR spectrometer with a Bruker CRYO platform accessory and the chemical shifts are referenced to TMS ($\delta = 0$) as an internal standard. FT-IR spectra were recorded on an Agilent Cary 600 spectrophotometer ($4000\text{--}650\text{ cm}^{-1}$) or a Perkin Elmer spectrophotometer ($4000\text{--}400\text{ cm}^{-1}$) with the samples compressed as KBr discs using a Specac press. Conductivities of the complexes were measured on a JENWAY 4520 conductivity meter at room temperature using freshly prepared solutions (1 mM) in MeOH. Electronic absorption spectra were recorded on a Shimadzu 2450 UV-visible spectrophotometer (190–1000 nm). Measurements of cyclic voltammetry were conducted with a PalmSense potentiostat (PSTrace 4.5 software) in MeCN under argon using a three-electrode electrochemical cell comprising a Pt-disc working electrode, a Pt-wire counter (auxiliary) electrode and a Ag/AgCl reference electrode with 0.1 M $[\text{Bu}_4\text{N}]\text{PF}_6$ as supporting electrolyte. Potentials are quoted with respect to that of the $\text{Cp}_2\text{Fe}^{0/+}$ couple ($E_{1/2} = 440\text{ mV vs. Ag/AgCl}$ under the experimental conditions) using ferrocene as an internal standard.

X-band EPR spectra were recorded on a Bruker ELEXSYS E-500 CW spectrometer (microwave frequency = 9.43 GHz). Variable-temperature magnetic susceptibility measurements were carried out on a Quantum Design EverCool SQUID magnetometer operating at an applied field of 8 kOe and palladium was used as the calibration standard. Diamagnetic corrections were performed the usual way using Pascal's constants. ^{57}Fe Mössbauer spectra were recorded on a conventional spectrometer with alternating current and constant acceleration of the γ -source ($^{57}\text{Co/Rh}$, 1.8 GBq), which was kept at room temperature. The minimum experimental line width was 0.24 mm s^{-1} (full width at half-height). The temperature of the sample was controlled with the aid of an Oxford Instruments Variox cryostat. Isomer shifts ($\delta / \text{mm s}^{-1}$) are quoted relative to $\alpha\text{-Fe}$ at room temperature. X-ray diffraction data were collected using a Bruker SMART APEX-II CCD diffractometer with graphite-monochromated Mo-K α radiation ($\lambda = 0.71073\text{ \AA}$). The structures were solved with the SHELXT^[65] software using intrinsic phasing and refined on F^2 with the SHELXL^[66] software using least squares minimization. The Olex2^[67] programme was used for molecular graphics and generation of publication material.

Acknowledgements

We owe a debt of gratitude to SQU Deanship of Research for financial support (IG/SCI/CHEM/19/04, MSS) and Deanship of Postgraduate Studies for a doctoral scholarship (MAA).

Conflict of Interest

The authors declare no conflict of interest.

Keywords

Ferric spin crossover · spin-transition plateau · noncovalent interactions · crystallographic phase transition · electronic and electrochemical processes

References

- [1] a) M. S. Haddad, W. D. Federer, M. W. Lynch, D. N. Hendrickson, *J. Am. Chem. Soc.* **1980**, *102*, 1468–1470; b) M. S. Haddad, M. W. Lynch, W. D. Federer, D. N. Hendrickson, *Inorg. Chem.* **1981**, *20*, 123–131.
- [2] A. Tissot, R. Bertoni, E. Collet, L. Toupet, M.-L. Boillot, *J. Mater. Chem.* **2011**, *21*, 18347–18353.
- [3] A. Tissot, P. Fertey, R. Guillot, V. Briois, M.-L. Boillot, *Eur. J. Inorg. Chem.* **2014**, 101–109.
- [4] A. I. Vicente, L. P. Ferreira, M. de D. Carvalho, V. H. N. Rodrigues, M. M. Dirtu, Y. Garcia, M. J. Calhorda, P. N. Martinho, *Dalton Trans.* **2018**, *47*, 7013–7019.
- [5] T. Boonprab, S. J. Lee, S. G. Telfer, K. S. Murray, W. Phonsri, G. Chastanet, E. Collet, E. Trzop, G. N. L. Jameson, P. Harding, D. J. Harding, *Angew. Chem. Int. Ed.* **2019**, *58*, 11811–11815; *Angew. Chem.* **2019**, *131*, 11937–11941.
- [6] W. Phonsri, P. Harding, L. Liu, S. G. Telfer, K. S. Marray, B. Moubaraki, T. M. Ross, G. N. L. Jameson, D. J. Harding, *Chem Sci.* **2017**, *8*, 3949–3959
- [7] N. Phukkaphan, D. L. Cruickshank, K. S. Murray, W. Phonsri, P. Harding, D. J. Harding, *Chem. Commun.* **2017**, *53*, 9801–9804.

- [8] S. Kang, Y. Shiota, A. Kariyazaki, S. Kanegawa, K. Yoshizawa, O. Sato, *Chem. Eur. J.* **2016**, *22*, 532–538.
- [9] T. Fujinami, M. Koike, N. Matsumoto, Y. Sunatsuki, A. Okazawa, N. Kojima, *Inorg. Chem.* **2014**, *53*, 2254–2259.
- [10] M. Nakaya, K. Shimayama, K. Takami, K. Hirata, A. S. Alao, M. Nakamura, L. F. Lindoy, S. Hayami, *Chem. Lett.* **2014**, *43*, 1058–1060.
- [11] D. J. Harding, W. Phonsri, P. Harding, I. A. Gass, K. S. Murray, B. Moubaraki, J. D. Cashion, L. Liu, S. G. Telfer, *Chem. Commun.* **2013**, *49*, 6340–6342.
- [12] S. Hayami, K. Hiki, T. Kawahara, Y. Maeda, D. Urakami, K. Inoue, M. Ohama, S. Kawata, O. Sato, *Chem. Eur. J.* **2009**, *15*, 3497–3508.
- [13] S. Dorbes, L. Valade, J. A. Real, C. Faulmann, *Chem. Commun.* **2005**, 69–71.
- [14] S. Hayami, Z. Gu, H. Yoshiki, A. Fujishima, O. Sato, *J. Am. Chem. Soc.* **2001**, *123*, 11644–11650.
- [15] S. Hayami, Z. Gu, M. Shiro, Y. Einaga, A. Fujishima, O. Sato, *J. Am. Chem. Soc.* **2000**, *122*, 7126–7127.
- [16] M. Griffin, S. Shakespeare, H. J. Shepherd, C. J. Harding, J.-F. Létard, C. Desplanches, A. E. Goeta, J. A. K. Howard, A. K. Powell, V. Mereacre, Y. Garcia, A. D. Naik, H. Müller-Bunz, G. G. Morgan, *Angew. Chem. Int. Ed.* **2011**, *50*, 896–900.
- [17] B. J. C. Vieira, J. T. Coutinho, I. C. Santos, L. C. J. Pereira, J. C. Waerenborgh, V. da Gama, *Inorg. Chem.* **2013**, *52*, 3845–3850.
- [18] D. J. Harding, W. Phonsri, P. Harding, K. S. Murray, B. Moubaraki, G. N. L. Jameson, *Dalton Trans.* **2015**, *44*, 15079–15082.
- [19] J. Tang, J. S. Costa, S. Smulders, G. Molnár, A. Bousseksou, S. J. Teat, Y. Li, G. A. van Albada, P. Gamez, J. Reedijk, *Inorg. Chem.* **2009**, *48*, 2128–2135.
- [20] D. J. Harding, D. Sertphon, P. Harding, K. S. Murray, B. Moubaraki, J. D. Cashion, H. Adams, *Chem. Eur. J.* **2013**, *19*, 1082–1090.
- [21] A. J. Conti, R. K. Chadha, K. M. Sena, A. L. Rheingold, D. N. Hendrickson, *Inorg. Chem.* **1993**, *32*, 2670–2680.

- [22] P. Gamez, J. S. Costa, M. Quesada, G. Aromi, *Dalton Trans.* **2009**, 7845–7853.
- [23] M. A. Halcrow, *Chem. Soc. Rev.* **2011**, *40*, 4119–4142.
- [24] R. H. Petty, E. V. Dose, M. F. Tweedle, L. J. Wilson, *Inorg. Chem.* **1978**, *17*, 1064–1071.
- [25] M. S. Haddad, W. D. Federer, M. W. Lynch, D. N. Hendrickson, *Inorg. Chem.* **1981**, *20*, 131–139.
- [26] P. G. Sim, E. Sinn, R. H. Petty, C. L. Merrill, L. J. Wilson, *Inorg. Chem.* **1981**, *20*, 1213–1222.
- [27] M. D. Timken, D. N. Hendrickson, E. Sinn, *Inorg. Chem.* **1985**, *24*, 3947–3955.
- [28] M. D. Timken, A. M. Abdel-Mawgoud, D. N. Hendrickson, *Inorg. Chem.* **1986**, *25*, 160–164.
- [29] S. Hayami, S. Miyazaki, M. Yamamoto, K. Hiki, N. Motokawa, A. Shuto, K. Inoue, T. Shinmyozu, Y. Maeda, *Bull. Chem. Soc. Jpn.* **2006**, *79*, 442–450.
- [30] W. Phonsri, D. J. Harding, P. Harding, K. S. Murray, B. Moubaraki, I. A. Gass, J. D. Cashion, G. N. L. Jameson, H. Adams, *Dalton Trans.* **2014**, *43*, 17509–17518.
- [31] B. de P. Cardoso, A. I. Vicente, J. B. J. Ward, P. J. Sebastião, F. V. Chávez, S. Barroso, A. Carvalho, S. J. Keely, P. N. Martinho, M. J. Calhorda, *Inorg. Chim. Acta* **2015**, *432*, 258–266.
- [32] A. I. Vicente, A. Joseph, L. P. Ferreira, M. de D. Carvalho, V. H. N. Rodrigues, M. Duttine, H. P. Diogo, M. E. M. da Piedade, M. J. Calhorda, P. N. Martinho, *Chem. Sci.* **2016**, *7*, 4251–4258.
- [33] F. F. Martins, A. Joseph, H. P. Diogo, M. E. M. da Piedade, L. P. Ferreira, M. D. Carvalho, S. Barroso, M. J. Romão, M. J. Calhorda, P. N. Martinho, *Eur. J. Inorg. Chem.* **2018**, 2976–2983.
- [34] a) M. S. Shongwe, B. A. Al-Rashdi, H. Adams, M. J. Morris, M. Mikuriya, G. R. Hearne, *Inorg. Chem.* **2007**, *46*, 9558–9568; b) K. D. Murnaghan, C. Carbonera, L. Toupet, M. Griffin, M. M. Dîrtu, C. Desplanches, Y. Garcia, E. Collet, J.-F. Létard, G. G. Morgan, *Chem. Eur. J.* **2014**, *20*, 5613–5618.
- [35] L. Pogány, B. Brachňáková, J. Moncol, J. Pavlik, I. Nemeč, Z. Trávníček, M. Mazúr, L. Bučinský, L. Suchánek, I. Šalitroš, *Chem Eur. J.* **2018**, *24*, 5191–5203.
- [36] G. R. Desiraju, R. Parthasarathy, *J. Am. Chem. Soc.* **1989**, *111*, 8725–8726.
- [37] T. T. T. Bui, S. Dahaoui, C. Lecomte, G. R. Desiraju, E. Espinosa, *Angew. Chem. Int. Ed.* **2009**, *48*, 3838–3841.

- [38] G. R. Desiraju, P. S. Ho, L. Kloo, A. C. Legon, R. Marquardt, P. Metrangolo, P. Poltzer, G. resnati, K. Rissanen, *Pure Appl. Chem.* **2013**, *85*, 1711–1713.
- [39] A. Mukherjee, S. Totladi, G. R. Desiraju, *Acc. Chem. Res.* **2014**, *47*, 2514–2524.
- [40] K. B. Ghiassi, J. Wescott, S. Y. Chen, A. L. Balch, M. M. Olmstead, *Cryst. Growth Des.* **2015**, *15*, 2480–2485.
- [41] G. Cavallo, P. Metrangolo, R. Milani, T. Pilati, A. Priimagi, G. Resnatti, G. Terraneo, *Chem. Rev.* , **2016**, *116*, 2478–2601.
- [42] B. Dey, S. Roy, J. Titiš, R. Boča, S. P. Bera, A. Mondal, S. Konar, *Inorg. Chem.* **2019**, *58*, 1134–1146.
- [43] C. Faulmann, K. Jacob, S. Dorbes, S. Lampert, I. Malfant, M.L. Doublet, L. Valade, J. A. Real, *Inorg. Chem.* **2007**, *46*, 8548–8559.
- [44] N. Ngah, N. Mohamad, M. Ahmad, B. M. Yamin, *Acta Cryst.* **2005**, *E61*, o969–o970.
- [45] M. S. Shongwe, U. A. Al-Zaabi, F. Al-Mjeni, C. S. Eribal, E. Sinn, I. A. Al-Omari, H. H. Hamdeh, D. Matoga, H. Adams, M. J. Morris, A. L. Rheingold, E. Bill, D. J. Sellmyer, *Inorg. Chem.* **2012**, *51*, 8241–8253.
- [46] M. S. Shongwe, S. H. Al-Rahbi, M. A. Azani, A. A. Al-Muharbi,, F. Al-Mjeni, D. Matoga, A. Gismelseed, I. A. Al-Omari,, A. Yousif, H. Adams, M. J. Morris, M. Mikuriya, *Dalton Trans.* **2012**, *41*, 2500–2514.
- [47] M. S. Shongwe, K. S. Al-Bahri, M. Mikuriya, H. Adams, M. J. Morris, E. Bill, K. C. Molloy, *Chem. Eur. J.* **2014**, *20*, 9693–9701.
- [48] C.-F. Sheu, S.-M. Chen, G.-H. Lee, Y.-H. Liu, Y.-S. Wen, J.-J. Lee, Y.-C. Chuang, Y. Wang, *Eur. J. Inorg. Chem.* **2013**, 894–901.
- [49] E. W. Y. Tido, C. Faulmann, R. Roswanda, A. Meetsma, P. J. van Koningsbruggen, *Dalton Trans.* **2010**, *39*, 1643–1651.
- [50] M. S. Shongwe, C. H. Kaschula, M. S. Adsetts, E. W. Ainscough, A. M. Brodie, M. J. Morris, *Inorg. Chem.* **2005**, *44*, 3070–3079.
- [51] D. Matoga, J. Szklarzewicz, K. Stadnicka, M. S. Shongwe, *Inorg. Chem.* **2007**, *46*, 9042–9044.
- [52] R. Pritchard, S. A. Barrett, C. A. Kilner, M. A. Halcrow, *Dalton Trans.* **2008**, 3159–3168.

- [53] M. Nihei, T. Shiga, Y. Maeda, H. Oshio, *Coord. Chem. Rev.* **2007**, *251*, 2606–2621.
- [54] M. Clemente-León, E. Coronado, M. López-Jordà, G. M. Espallargas, A. Soriano-Portillo, J. C. Waerenborgh, *Chem. Eur. J.* **2010**, *16*, 2207–2219.
- [55] N. Arulsamy, D. J. Hodgson, *Inorg. Chem.* **1994**, *33*, 4531–4536.
- [56] a) C. Hansch, A. Leo, R. W. Taft, *Chem. Rev.* **1991**, *91*, 161–191; b) https://en.wikipedia.org/wiki/Hammett_equation
- [57] B. P. Gaber, V. Miskowski, T. G. Spiro, *J. Am. Chem. Soc.* **1974**, *96*, 6868.
- [58] C. Imbert, H. P. Hratchian, M. Lanznaster, M. J. Heeg, L. M. Hryhorczuk, B. R. McGarvey, H. B. Schlegel, C. N. Verani, *Inorg. Chem.* **2005**, *44*, 7414–7422.
- [59] M. Lanznaster, A. Neves, A. J. Bortoluzzi, A. M. C. Assumpção, I. Vencato, S. P. Machado, S. M. Drechsel, *Inorg. Chem.* **2006**, *45*, 1005–1011.
- [60] R. Kannappan, S. Tanase, I. Mutikainen, U. Turpeinen, J. Reedijk, *Polyhedron*, **2006**, *25*, 1646–1654.
- [61] S. G. Sreerama, A. Mukhopadhyay, S. Pal, *Inorg. Chem. Commun.* **2006**, *9*, 1083–1086.
- [62] A. K. Patra, M. M. Olmstead, P. K. Mascharak, *Inorg. Chem.* **2002**, *41*, 5403–5409.
- [63] a) D. Boinnard, A. Bousseksou, A. Dworkin, J.-M. Savariault, F. Varret, J.-P. Tuchagues, *Inorg. Chem.* **1994**, *33*, 271–281; b) L. Salmon, A. Bousseksou, B. Donnadieu, J.-P. Tuchagues, *Inorg. Chem.* **2005**, *44*, 1763–1773.
- [64] M. M. Allard, J. A. Sonk, M. J. Heeg, B. R. McGarvey, H. B. Schlegel, C. N. Verani, *Angew. Chem. Int. Ed.* **2012**, *51*, 3178–3182.
- [65] G. M. Sheldrick, *Acta Cryst.* **2015**, *A71*, 3–8.
- [66] G. M. Sheldrick, *Acta Cryst.* **2008**, *A64*, 112–122.
- [67] O. V. Dolomanov, L. J. Bourhis, R. J. Gildea, J. A. K. Howard, H. Puschmann, *J. Appl. Cryst.* **2009**, *42*, 339–341.

TABLES

Accepted Manuscript

Table 1. Selected crystallographic data for [Fe^{III}(5-F-salMeen)₂]ClO₄, [Fe^{III}(5-Cl-salMeen)₂]ClO₄, [Fe^{III}(5-Br-salMeen)₂]ClO₄ and [Fe^{III}(5-I-salMeen)₂]ClO₄.

	[Fe ^{III} (5-F-salMeen) ₂]ClO ₄ (1)		[Fe ^{III} (5-Cl-salMeen) ₂]ClO ₄ (2)		[Fe ^{III} (5-Br-salMeen) ₂]ClO ₄ (3)		[Fe ^{III} (5-I-salMeen) ₂]ClO ₄ (4)	
Chemical formula	C ₂₀ H ₂₄ ClF ₂ FeN ₄ O ₆		C ₂₀ H ₂₄ Cl ₃ FeN ₄ O ₆		C ₂₀ H ₂₄ Br ₂ ClF ₂ FeN ₄ O ₆		C ₂₀ H ₂₄ ClI ₂ FeN ₄ O ₆	
Molar Mass (g/mol)	545.73	545.73	578.63	578.63	667.55	667.55	761.53	761.53
<i>T</i> (K)	90	298	90	273	90	298	90	298
Crystal system	Monoclinic	Monoclinic	Monoclinic	Monoclinic	Monoclinic	Monoclinic	Monoclinic	Monoclinic
Space group	<i>P</i> 2 ₁ / <i>n</i>	<i>P</i> 2 ₁ / <i>n</i>	<i>P</i> 2 ₁ / <i>n</i>	<i>P</i> 2 ₁ / <i>n</i>	<i>P</i> 2 ₁ / <i>n</i>	<i>P</i> 2 ₁ / <i>n</i>	<i>P</i> 2 ₁ / <i>n</i>	<i>P</i> 2 ₁ / <i>n</i>
<i>a</i> (Å)	11.0849(16)	11.3206(15)	10.9575(15)	11.2263(5)	10.894(3)	11.130(3)	10.3866(5)	10.8391(16)
<i>b</i> (Å)	23.944(4)	24.132(3)	24.553(3)	24.4985(10)	24.853(7)	24.808(6)	25.1537(12)	25.262(4)
<i>c</i> (Å)	17.603(3)	17.714(2)	18.105(2)	18.3001(8)	18.663(5)	18.790(5)	19.5934(10)	19.748(3)
<i>α</i> (deg)	90	90	90	90	90	90	90	90
<i>β</i> (deg)	102.872(2)	100.733(2)	101.320(2)	99.3670(10)	100.767(4)	99.152(4)	99.9580(10)	98.567(3)
<i>γ</i> (deg)	90	90	90	90	90	90	90	90
<i>V</i> (Å ³)	4554.8(11)	4754.4(11)	4776.3(11)	4965.9(4)	4964(2)	5122(2)	5157.2(4)	5347.1(13)
<i>Z</i>	8	8	8	8	8	8	8	8
<i>ρ</i> _{calc} (g/cm ³)	1.592	1.525	1.609	1.548	1.787	1.731	1.958	1.892
<i>μ</i> (mm ⁻¹)	0.841	0.806	1.012	0.973	3.979	3.856	3.119	3.014
<i>F</i> (000)	2248	2248	2376	2376	2664	2664	2952	2952
Crystal size (mm)	0.240 × 0.190 × 0.110	0.320 × 0.160 × 0.140	0.400 × 0.250 × 0.150	0.300 × 0.240 × 0.220	0.430 × 0.220 × 0.150	0.430 × 0.220 × 0.150	0.300 × 0.200 × 0.180	0.200 × 0.080 × 0.050
<i>θ</i> range (deg)	1.701-27.500	1.688-27.500	2.178-28.540	1.662-27.497	1.639-27.500	1.642-27.499	1.929-28.488	2.027-27.500
Reflns collected	28032	30280	31307	31670	29229	30613	33766	34212
<i>R</i> _{int}	0.0920	0.0758	0.0494	0.0358	0.0561	0.0535	0.0316	0.1005
GOF on <i>F</i> ²	1.047	0.960	0.834	0.995	0.936	0.792	0.832	1.063
<i>R</i> ₁ , <i>wR</i> ₂ [<i>I</i> > 2σ(<i>I</i>)]	0.0662, 0.1058	0.0612, 0.1479	0.0423, 0.1140	0.0527, 0.1410	0.0588, 0.1337	0.0579, 0.1313	0.0399, 0.1089	0.0868, 0.1516
<i>R</i> ₁ , <i>wR</i> ₂ (All data)	0.1367, 0.1302	0.1519, 0.2094	0.0718, 0.1345	0.0865, 0.1736	0.1119, 0.1472	0.1556, 0.1512	0.0548, 0.1214	0.2069, 0.2012

Table 2 Selected crystallographic data for [Fe^{III}(5-Cl-salMeen)₂]BPh₄·2MeOH (**5**)

	90 K	298 K
Chemical formula	C ₄₆ H ₅₂ BCl ₂ FeN ₄ O ₄	C ₄₆ H ₅₂ BCl ₂ FeN ₄ O ₄
Molar Mass (g/mol)	862.47	862.47
Crystal system	Monoclinic	Orthorhombic
Space group	<i>P</i> 2 ₁	<i>C</i> 222 ₁
<i>a</i> (Å)	11.467(2)	14.4983(17)
<i>b</i> (Å)	16.723(3)	18.238(2)
<i>c</i> (Å)	11.482(2)	16.819(2)
<i>α</i> (deg)	90	90
<i>β</i> (deg)	102.727(3)	90
<i>γ</i> (deg)	90	90
<i>V</i> (Å ³)	2147.7(7)	4447.4(9)
<i>Z</i>	2	4
ρ_{calc} (g/cm ³)	1.334	1.288
μ (mm ⁻¹)	0.524	0.506
<i>F</i> (000)	906	1812
Crystal size (mm)	0.380 × 0.350 × 0.180	0.380 × 0.350 × 0.180
θ range (deg)	1.218–27.496	2.541–27.499
Reflns collected	13641	14339
<i>R</i> _{int}	0.0397	0.0572
GOF on <i>F</i> ²	1.036	1.029
<i>R</i> ₁ , <i>wR</i> ₂ [<i>I</i> > 2σ(<i>I</i>)]	0.0464, 0.0898	0.0614, 0.1368
<i>R</i> ₁ , <i>wR</i> ₂ (All data)	0.0542, 0.0933	0.0960, 0.1504

Table 3. Halogen-halogen interactions in [Fe(5-X-salMeen)₂]ClO₄

Compound	X...X Contacts	Distance (Å)	θ ₁ (°)	θ ₂ (°)
T = 298 K				
[Fe(5-Br-salMeen) ₂]ClO ₄	Br2...Br4	3.493	165.15	88.34
[Fe(5-I-salMeen) ₂]ClO ₄	I2...I3	3.779	168.35	84.87
T = 90 K				
[Fe(5-Cl-salMeen) ₂]ClO ₄	Cl1...Cl4	3.267	168.63	93.67
[Fe(5-Br-salMeen) ₂]ClO ₄	Br1...Br2	3.400	169.51	89.94
[Fe(5-I-salMeen) ₂]ClO ₄	I1...I4	3.704	171.88	82.89

Table 4. Selected bond distances (Å), angles (°) and distortion parameters (°) in the coordination spheres of [Fe^{III}(5-X-salMeen)₂ClO₄] (1–4)

	1	2*	3	4
T = 298 K				
<i>Complex cation 1</i>				
Fe1–O _{ph}	1.910(3)	1.917(3)	1.913(4)	1.927(5)
Fe1–O _{ph}	1.919(3)	1.932(2)	1.943(4)	1.941(4)
Fe1–N _{im}	2.091(4)	2.103(3)	2.096(5)	2.103(5)
Fe1–N _{im}	2.093(4)	2.105(3)	2.116(5)	2.109(5)
Fe1–N _{am}	2.179(4)	2.192(3)	2.195(5)	2.192(5)
Fe1–N _{am}	2.190(4)	2.201(3)	2.196(5)	2.195(5)
Σ	71.7	73.6	73.2	71.3
Θ _{im-am}	78.1, 78.4	78.2, 77.9	78.0, 78.2	78.1, 78.0
<i>Complex cation 2</i>				
Fe2–O _{ph}	1.919(3)	1.912(2)	1.917(4)	1.914(5)
Fe2–O _{ph}	1.929(3)	1.919(3)	1.918(4)	1.956(5)
Fe2–N _{im}	2.096(4)	2.100(3)	2.090(5)	2.118(5)
Fe2–N _{im}	2.104(4)	2.101(3)	2.103(5)	2.126(6)
Fe2–N _{am}	2.197(4)	2.171(3)	2.167(5)	2.198(5)
Fe2–N _{am}	2.206(4)	2.192(3)	2.180(5)	2.215(6)
Σ	74.0	70.5	71.6	76.4
Θ _{im-am}	78.3, 77.8	78.1, 78.4	77.9, 78.1	77.4, 78.1
T = 90 K				
<i>Complex cation 1</i>				
Fe1–O _{ph}	1.925(3)	1.9268(19)	1.928(4)	1.924(3)
Fe1–O _{ph}	1.929(3)	1.9313(18)	1.935(4)	1.935(3)
Fe1–N _{im}	2.094(3)	2.112(2)	2.119(5)	2.103(3)
Fe1–N _{im}	2.098(4)	2.113(2)	2.123(5)	2.104(3)
Fe1–N _{am}	2.182(4)	2.189(2)	2.188(5)	2.179(3)
Fe1–N _{am}	2.202(4)	2.196(2)	2.205(6)	2.189(3)
Σ	68.8	70.4	71.3	72.9
Θ _{im-am}	78.3, 78.0	78.4, 77.9	78.3, 78.2	78.3, 78.1
<i>Complex cation 2</i>				
Fe2–O _{ph}	1.877(3)	1.8769(18)	1.871(4)	1.875(3)
Fe2–O _{ph}	1.881(3)	1.8831(17)	1.892(4)	1.886(3)
Fe2–N _{im}	1.937(3)	1.935(2)	1.953(5)	1.936(3)
Fe2–N _{im}	1.937(3)	1.937(2)	1.959(5)	1.941(3)
Fe2–N _{am}	2.032(3)	2.034(2)	2.043(5)	2.033(3)
Fe2–N _{am}	2.034(4)	2.036(2)	2.050(5)	2.039(3)
Σ	52.7	53.1	53.6	55.2
Θ _{im-am}	83.4, 83.1	83.4, 83.0	83.1, 83.1	83.5, 82.9

Σ = sum of the deviations of the *cis* angles from the right angle; Θ_{im-am} = the chelate angle for the –CH=NCH₂CH₂NHR ligand fragment; *Higher temperature for complex 2 = 273 K.

Table 5. Selected bond distances (Å), angles (°) and distortion parameters (°) in the coordination spheres of [Fe^{III}(5-Cl-salMeen)₂]BPh₄·2MeOH

	298K	90 K
Fe1–O1	1.852(4)	1.855(5)
Fe1–O1		1.874(5)
Fe1–N1	1.921(4)	1.931(5)
Fe1–N3		1.924(5)
Fe1–N2	2.037(5)	2.051(6)
Fe1–N4		2.039(6)
Σ	39.9	41.7
Θ _{im-am}	83.7	83.7, 83.4
<i>Trans</i> angles	178.72, 176.72, 176.72	178.3, 176.5, 176.4

Table 6: Electronic effects and electrochemical data for $[\text{Fe}^{\text{III}}(5\text{-X-salMeen})_2]\text{ClO}_4$ (X = H, F, Cl, Br, I).

$[\text{Fe}^{\text{III}}(5\text{-X-salMeen})_2]\text{ClO}_4$ (<i>p</i> -X-phenol)	pK_a	σ_p	$E_{1/2}$ (mV)	ΔE_p (mv)	χ (H or X)
$[\text{Fe}^{\text{III}}(\text{salMeen})_2]\text{ClO}_4$	9.99	0.00	-0.39	86.7	2.1
$[\text{Fe}^{\text{III}}(5\text{-F-salMeen})_2]\text{ClO}_4$ (1)	9.89	0.06	-0.35	78.5	4.0
$[\text{Fe}^{\text{III}}(5\text{-Cl-salMeen})_2]\text{ClO}_4$ (2)	9.41	0.23	-0.30	73.3	3.0
$[\text{Fe}^{\text{III}}(5\text{-Br-salMeen})_2]\text{ClO}_4$ (3)	9.37	0.23	-0.29	73.6	2.8
$[\text{Fe}^{\text{III}}(5\text{-I-salMeen})_2]\text{ClO}_4$ (4)	9.33	0.28	-0.28	73.6	2.5